Working Report 2016-52

Parametrisation of Fractures – PUSH Test Execution and Back-Analysis

Jouni Valli, Matti Hakala
Johannes Suikkanen, Jussi Mattila
Juha Heine
Charlotta Simelius

October 2016

POSIVA OY
Olkiluoto
FI-27160 EURAJOKI, FINLAND
Phone (02) 8372 31 (nat.), (+358-2-) 8372 31 (int.)
Fax (02) 8372 3809 (nat.), (+358-2-) 8372 3809 (int.)

Working Report 2016-52

Parametrisation of Fractures – PUSH Test Execution and Back-Analysis

Jouni Valli, Matti Hakala
KMS Hakala Oy

Johannes Suikkanen, Jussi Mattila
Posiva Oy

Juha Heine
SMCOY

Charlotta Simelius
Pöyry Finland Oy

October 2016

Working Reports contain information on work in progress
or pending completion.

ABSTRACT

An *in situ* push test of a fracture surface under constant normal stiffness (CNS) conditions was conducted at a depth of 437 meters in the ONKALO underground research facility. The objective of the experiment was to study the *in situ* shear strength of fracture surfaces at an easily accessible location, with a simple associated geometry, under low normal force and large shear displacement. The push test was conducted to assess the methodology of conducting an *in situ* shear test and to gain knowledge of the shear behaviour of fractures at the site.

Loose blocks surrounding the tunnel opening are formed when natural fracture surfaces intersect the excavation surface of the tunnel. The targeted block is limited by a steep, North-South-orientated Riedel-fracture related to the BFZ-300 geological feature in the ONKALO Parking Hall.

This working report describes the experiment procedure of the push test and analysis of the measured results. The displacement and rotation during the push test were monitored by LVDT-sensors, while the normal- and shear forces were measured using load cells and a hydraulic pressure gauge. Fracture parameters were initially estimated according to the Q-classification system along with JRC evaluation. The test response and these selected parameter values were then back analysed with iterative rock mechanics simulations using the three-dimensional distinct element code 3DEC.

Back-analysis using 3DEC was performed through a step-wise approach in order to avoid numerical convergence problems and to study the effect of geometry on results. The three fracture surfaces modelled were a planar fracture surface, a fully-mated coarse surface and an unmated coarse surface. The shear and normal stress measurements from the shear test experiment were compared to those from the different models run with different parameters, based on the originally estimated fracture surface area. The unmated model was found to yield an acceptable match using an initial friction angle of 47° and a residual friction angle of 40°, although underestimating the initial peak strength after 2 - 5 mm shear. This peak was most likely associated with upper side areas of the block broken off during the initial peak. These details were not included in the model geometry. Most importantly a low constant normal stiffness condition was found to increase shear resistance by over 30% from the initial peak to final shear displacement of 34 mm. The back-analysed friction angles are about 10° greater than those observed from small scale laboratory tests. This suggests that the scale effect where longer fractures exhibit a lower shear resistance normally assumed in practice, may not be valid for the repository rock mass under study.

Findings from this study revealed the following: (1) Displacement control should be used to prevent rotation of the block. (2) Anchor bolts should be fully grouted with proper setup using I-beams to eliminate any effect from the bending of the bolts. (3) Normal displacement should be measured in multiple locations. (4) Finally, the test setup should be able to generate high normal stress to mimic constant normal stiffness resulting from confined *in situ* conditions at 450 m depth.

Keywords: ONKALO, fracture, in situ, shear test, stiffness, numerical, back analyses.

RAKOJEN PARAMETRISOINTI PROJEKTI - PUSH KOKEEN SUORITTAMINEN JA TAKAISINLASKENNAT

TIIVISTELMÄ

Työssä on kuvattu vakionormaalijäykkyysolosuhteissa (constant normal stiffness, CNS) suoritettu in situ rakoleikkauskoe, joka toteutettiin Posiva Oy:n ONKALO tutkimustilassa 437 m syvyydellä. Tarkoituksena oli mitata rakopinnan in situ leikkausvastusta alhaisella normaalikuormalla suuren leikkaussiirtymän aikana. Koegeometrian tuli olla yksinkertainen, helposti instrumentoitava ja mallinnettava. Tavoitteena oli saada tietoa raon käyttäytymisestä in situ olosuhteissa sekä hankkia kokemuksia tähän soveltuvasta koejärjestelystä.

Testiin soveltuvia lohkoja syntyy, kun luonnollinen kalliorako leikkaa tunnelin seinän pienellä kulmalla. Testikohteessa etelä-/pohjoissuuntainen, pystykaateinen hauraan murtuman vyöhykkeeseen ONK-BFZ300 liittyvä Riedel-rako, leikkaa ONKALOn pysäköintihallin.

Työssä on kuvattu yksityiskohtaisesti testauksen vaiheet ja mittaustulosten analysointi. Kokeen aikana raon kalliotilan puoleisen lohkon leikkaussiirtymää ja kiertymää seurattiin LVDT-antureilla, normaalivoimaa voima-antureilla ja leikkausvoimaa painelähettimellä. Alustavasti raon mekaaniset ominaisuudet arvioitiin Q-kalliolaatuluokituksen parametrien sekä raon karheutta kuvaavan JRC-luvun perusteella. Lopulliset rakoparametriarvot määritettiin iteratiivisilla kalliomekaanisilla simuloinneilla, jotka tehtiin kolmedimensionaalisella epäjatkuvan materian numeerisella menetelmällä 3DEC.

Simulointimallien realistisuutta tarkennettiin vaiheittain, jotta mallinnetun rakogeometrian vaikutus tulokseen olisi selvempi ja että mahdolliset numeeriset ongelmat pystyttiin hallitsemaan paremmin. Rakopinnasta tehtiin kolme mallia; tasomainen sekä karkeasti kolmioidut, vain toisen rakopuolen mukaiset täysin yhteensopivat ja molempien puolien mukaiset epäyhteensopivat pinnat. Mallien ja parametrien toimivuutta arvioitiin vertaamalla mitattuja raon leikkaus- ja normaalijännityksiä simulointimalleilla saatuihin vastaaviin arvoihin. Epäyhteensopivat pinnat antoivat parhaan tuloksen kitkakulman alkuarvolla 47° ja jäännösarvolla 40°. Simulointi aliarvioi 2 - 5 mm leikkaussiirtymällä havaittua ensimmäistä huippua, joka todennäköisesti liittyy työnnetyn lohkon reunasta kokeen alkuvaiheessa lohjenneisiin osiin, joita ei mallinnettu. Keskeisimpiä tuloksia oli, että leikkausvastus kasvoi yli 30% ensimmäisestä huipustaan, kun leikkausta jatkettiin 34 mm saakka. Jälkianalyysin mukaiset kitkakulmat olivat myös noin 10° suurempia kuin pienillä rakonäytteillä laboratoriokokeissa saatavat arvot. Edellä esitetyn perusteella yleisesti käytetty mittakaavaolettamus, jossa leikkausvastus(jännitys) pienenee rakopinnan kasvaessa, ei välttämättä pidä paikkaansa tutkitulle loppusijoituspaikan raolle.

Koejärjestelyn osalta havaittiin, että 1) kiertymisen estämiseksi leikkauskoetta tulee ohjata leikkaussiirtymällä. 2) normaalivoiman tarkentamiseksi lohkon normaalijännityksen antavat pultit tulee juottaa kallioon sementillä ja pulttien taipuman ehkäisemiseksi normaalivoima pitää välittää leikattavaan lohkoon I-palkin ja laakeroinnin välityksellä. 3) lohkon raon normaalin suuntaista siirtymää (dilataatio) tulee mitata

useassa pisteessä. 4) koejärjestelyn normaalivoiman kesto pitää suunnitella niin suureksi, että leikkauskokeen olosuhteet saadaan vastaamaan 450 m syvyydellä vallitsevaa vakionormaalijäykkyyttä.

Avainsanat: ONKALO, rako, in situ, leikkauskoe, jäykkyys, numeerinen, jälkianalyysi.

TABLE OF CONTENTS

1 INTRODUCTION

1.1 Introduction

ONKALO is an underground research facility at the Olkiluoto site in western Finland. ONKALO extends approximately to a depth of -450 meters and has provided a significant amount of research data regarding the final disposal of spent nuclear fuel in hard rock conditions. However, the insufficient amount of knowledge regarding the *in situ* shear strength of large fractures during large shear displacement has resulted in the planning of a PUSH test of a fracture surface at a tunnel wall.

This working report describes the experiment procedure of the PUSH test conducted for the BFZ - 300 fracture surface located at a depth of -437 m in ONKALO. The PUSH test was a supplementary study related to the POST-project performed as a collaborative effort by Posiva, SKB and NWMO. The aim of the POST project is fracture characterization for producing relevant rock mechanics parameters to enable modelling of post glacial earthquake scenarios. Characterising fractures and their parameterisation is essential for site description, optimizing repository layout, maximizing long-term safety and minimizing waste disposal costs. The PUSH test presented in this report has been conducted before the prediction calculations of the POST-project laboratory- and *in situ* test experiment campaign. The test produces information about fracture activation and shearing of a fracture with simple characteristics and geometry during large shear displacement up to 35 mm under low constant normal stiffness (CNS) conditions. Simple characteristics refer to the fairly uniform fracture features wherein fracture filling thickness and type do not vary notably across the surface. Geometry refers to the fact that it is a single fracture without any fracture splays.

The main objectives of the work presented in this report are:

- Performing an *in situ* shear test with a CNS boundary condition
- Validation of the simulation methodology developed for *in situ* shear tests (Valli & Hakala 2016a)
- Verifying that the observed behaviour from test execution matches the assumed behaviour
- Estimation of fracture shear strength and deformation parameters using back-analysis

2 FRACTURE SURFACE DESCRIPTION IN DRILL CORE

The targeted fracture for the PUSH test is a steep dipping fracture surface located behind a daylighted rock block in the southwestern corner of the ONKALO Parking Hall, indicated in Figure 2-1 and Figure 2-2. An overview of the test block and experiment setup is illustrated in Figure 2-3.

The target fracture is part of the BFZ-300 feature, which intersects the Parking Hall of ONKALO. The fracture is a Riedel-fracture of a fault and has been dextrally sheared in several geological phases. It has formed in the brittle reactivation phase (Aaltonen *et al.* 2016). The fracture surface has an average dip of 82° oriented towards the west. Geologically, the surrounding rock mass at the test site mainly consists of pegmatite leucosome in gneissic rock. The test block is largely veined gneiss (VGN), with some mica gneiss (MGN) or pegmatitic granite (PGR) apparent.

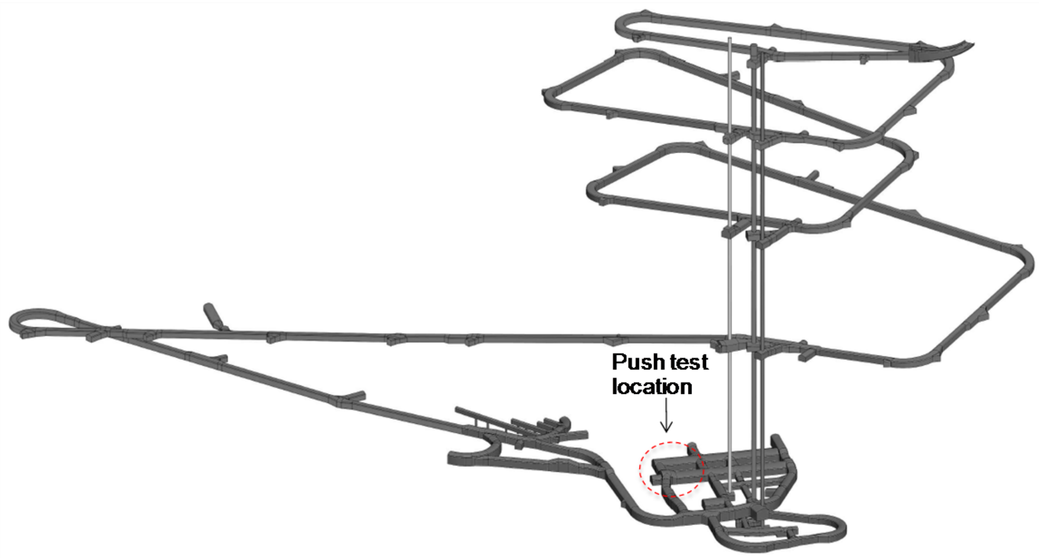

Figure 2-1. *The location of the test in the ONKALO facility.*

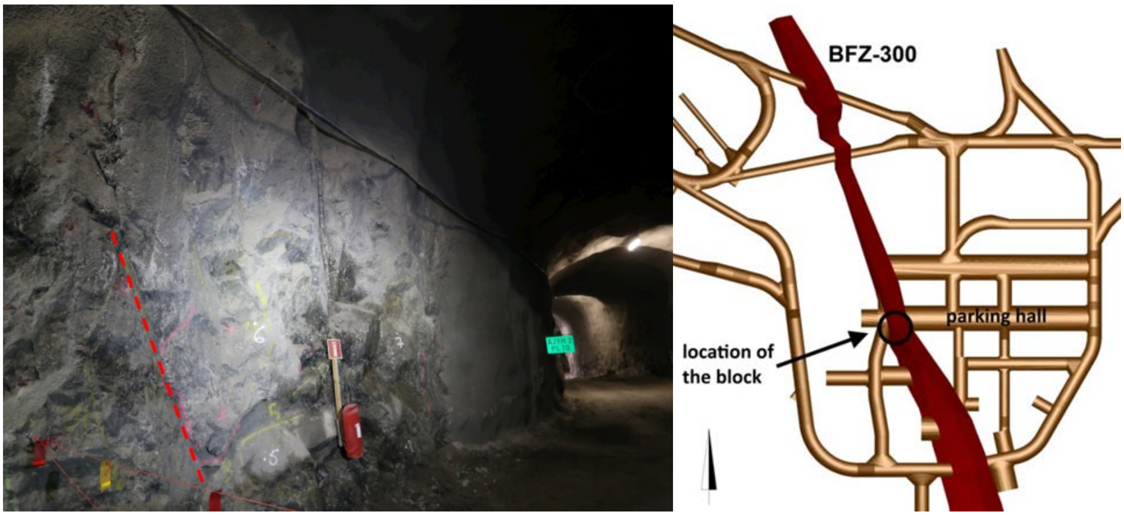

Figure 2-2. *Test area before the experiment (right) and the location of the test block (left). The loose block is delimited by a fracture on its left side (red dashed line).*

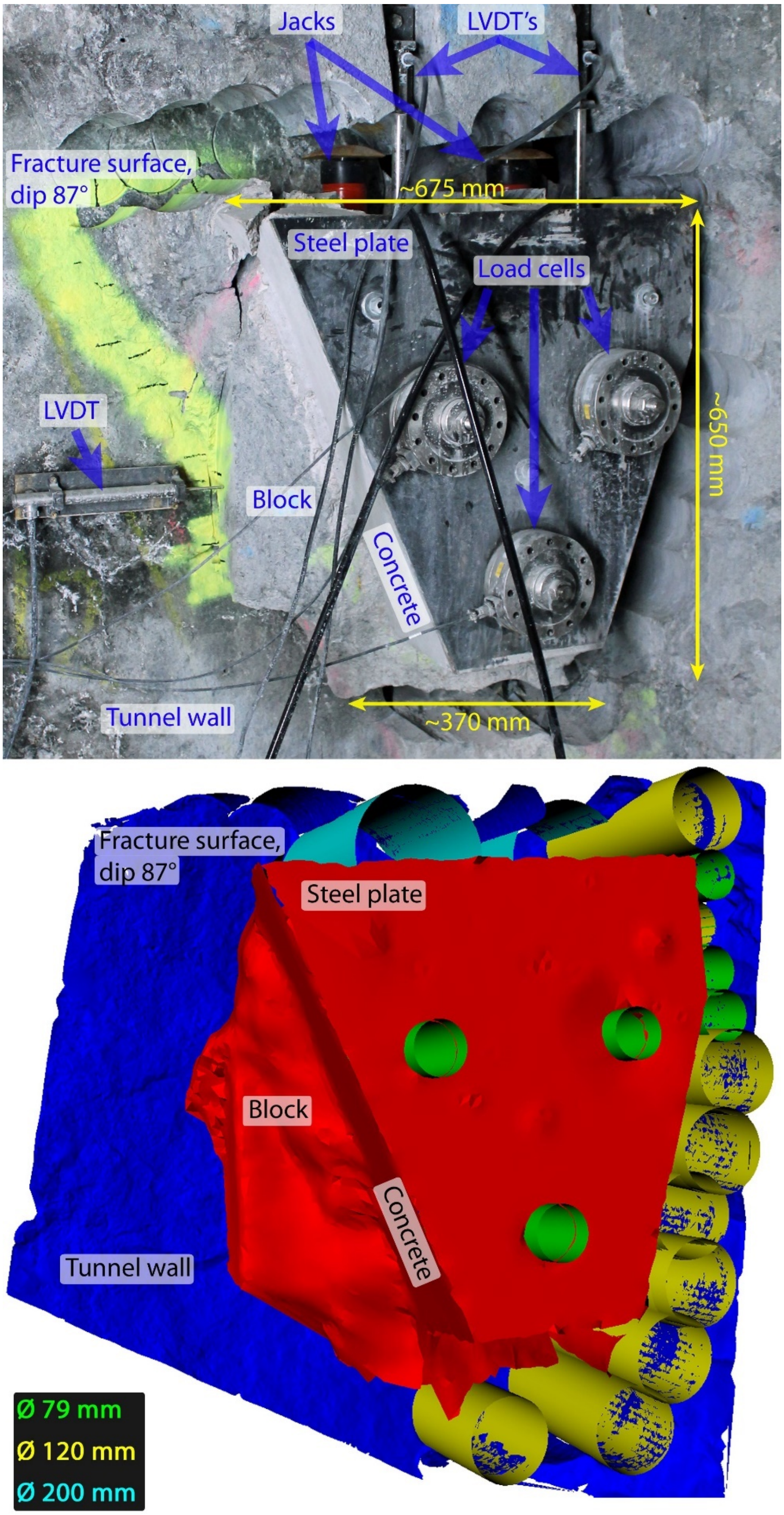

Figure 2-3. *Above: the test block after testing with approximate dimensions. Below: the test block based on photogrammetry, with colour-coded diameters for holes.*

The fracture surface at the test location was mapped as part of site characterization. Before the PUSH test, two ∅ 200 mm cores were drilled to intersect the fracture surface (Figure 2-4). The fracture profile was found to be rough and undulating, with an estimated J_r value of 3 according to the Q-classification system and a JRC_{100} value of 9 (Barton 2002). The fracture is a Riedel-fracture and exhibits evidence of shear.

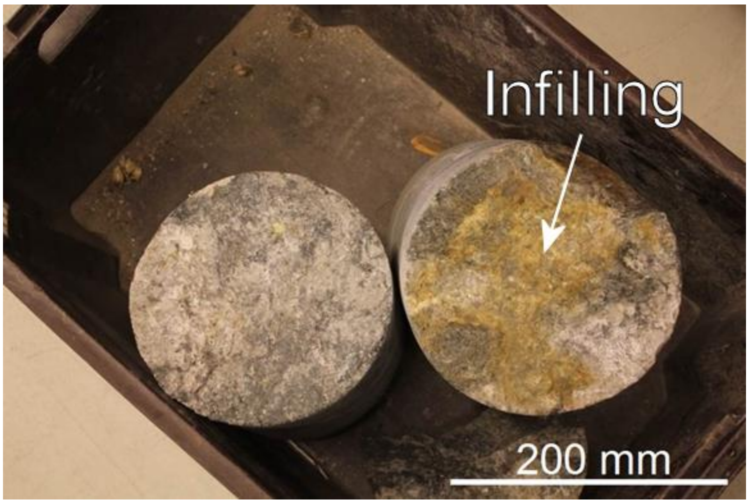

Figure 2-4. *Core samples drilled from the test location that depicts the quality of the fracture surface. Infilling of the fracture can be seen on the core on the right.*

From the drill core, the fracture surface exhibits a 0.2 mm thick filling layer consisting mainly of chlorite and kaolinite. The J_a value (a measure of the alteration of the fracture surface) was assigned a value of 3, due to extremely thin and non-softening mineral filling. Based solely on the core, the fracture was considered to be partially open.

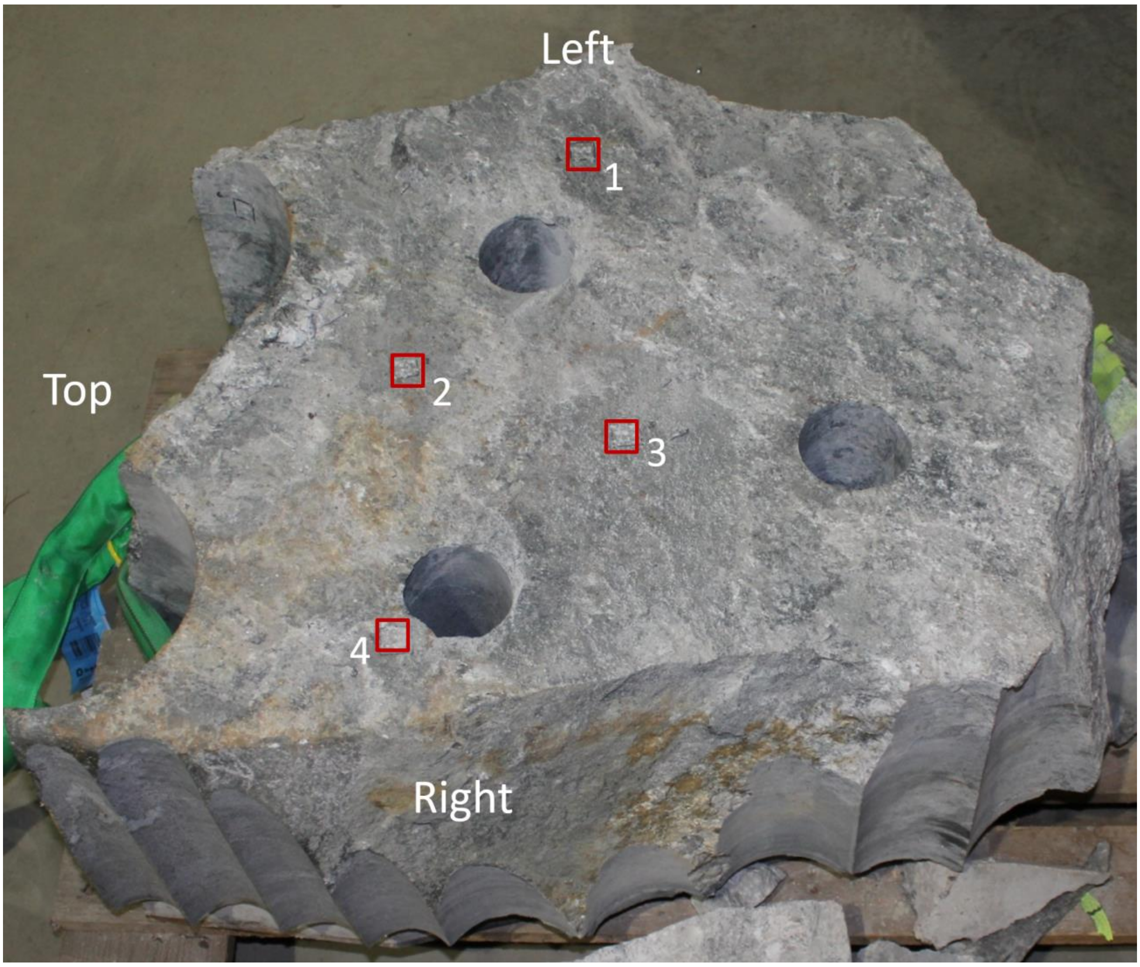

Figure 2-5. *Schmidt hammer measurement locations, as obtained from the fracture surface after execution of the PUSH test.*

Schmidt hammer testing was conducted at four points on the fracture surface and at two fresh reference points after execution of the PUSH test, with all of the points located in veined gneiss (VGN). The average rebound value (R) for the fracture surface was 59 and 53 for the reference rock (Figure 2-5). No other test data has been obtained from the location. The mean unconfined peak strength of intact rock of the equivalent rock type of the sampled core based on earlier ONKALO data is 108 MPa and the indirect tensile strength is 12.1 MPa (Posiva 2013). The initial mean cohesion and friction angle for fractures in VGN have been interpreted as 0.34 MPa and 29.5° and corresponding residual values are 0.16 MPa and 29.3° (Valli & Hakala 2016b).

3 EXPERIMENT DESCRIPTION

3.1 General experiment design

The experiment procedure consists of the test preparation including drilling of fracture samples and the execution of the *in situ* PUSH test. The initial and post-experiment conditions are illustrated in Figure 3-1 along with test dimensions. Test dimensions are described in detail in the following section.

The progression of the experiment:

1) Fracture selection
2) Coring of 2 holes for characterisation and instrumentation purposes
3) Drilling of three bolt holes and installation of anchors for Constant Normal Stiffness boundary condition (controlled by mechanically anchored bolts)
4) Installation of normal and shear displacement monitoring LVDT
5) Slot drilling for block release, and measruement of displacement during the block release
6) Block shear with measurement of vertical displacement and shear rotation

3.2 Experiment preparation

Prior to beginning experiment preparation, two rock bolts were also installed above the test block to improve work safety and confirm the stability of the remaining block. At this point the weight of the test block and the area of the original fracture surface was *estimated* to be 325 kg and 0.319 m^2 on the fracture side of the block.

Preparation proceeded according to the following progression:

Steel plate installation

A 15 mm thick steel plate with three 79 mm diameter holes was mechanically anchored to the test block, after which the void formed between the rock block and the steel plate was backfilled with concrete. Three pipes were installed through the steel slab holes in order to prevent concrete spilling into the anchor bolt holes during casting. Three ∅ 15 mm expansion anchors were installed in the rock and were tensioned to ensure full contact between the concrete layer, rock and the steel plate during casting. The thickness of the concrete layer varied between 7.5 and 13 cm, as tabulated in Figure 3-2.

Drilling

Two ∅ 200 mm holes were then drilled to obtain rock samples through the fracture surface above the block and creating positions for jacks to be used to induce shear (Figure 3-2, holes 1 and 2).Three ∅ 62 mm holes were drilled through the block extending to a depth of 1000 mm from the fracture surface, noted as holes 3 to 5 in Figure 3-2. The holes were enlarged eccentrically within the block to a diameter of 79 mm to allow for at least 30 mm vertical displacement of the fracture surface without bolt and rock contact.

Bolting

Three mechanically anchored bolts with a diameter of 20 mm were then installed in holes 3 – 5. The bolt steel grade was EN 1.4301, with a yield capacity of 190 MPa (60 kN) and an ultimate capacity 500 MPa (157 kN). When tested, anchor capacities were determined to be ca. 100 kN.

Dimensions

The depths to the bolt anchors when measured from the surface of the 15 mm thick steel plate located on top of the loose block were 1270, 1280 and 1290 mm for the left, right and bottom bolt holes, respectively. Anchorage length was 70 mm. The thickness of the bolt faceplates on top of the steel baseplate of the block was 15 mm. The load cells on top the bolt baseplates were 42 mm thick. Both bolt faceplates and the load cells were 150 mm in diameter. ∅ 60 mm washers with a thickness of 15 mm were located on top of the load cells (Figure 3-1).

LVDT installation

Grooves for Linear Variable Differential Transducer (LVDT) sensors (see section 3.3) were sawn into the tunnel wall to enable the monitoring of displacement at three locations: two above the block to measure vertical displacement and one on the left side of the block to measure rotation.

Instrumentation

After installation of the LVDT sensors two hydraulic jacks (Figure 3-3), with an individual capacity of 25 tons, were then set into the formerly drilled ∅ 200 mm sample holes (holes 1 and 2 in Figure 3-2) to produce the necessary shear force along the fracture surface during the execution of the experiment. Concave steel baseplates (Figure 3-3) were used to provide even surfaces for the jacks both above and below the jacks. The jacks were installed parallel to the fracture surface in order to minimize out of plane shear forces, as shown in Figure 3-4.

Block release

After instrumentation of the block, excluding the LVDT-sensors installed earlier, the block was released by slot drilling according to the plan shown in Figure 3-5. The LVDT sensors were used to monitor the block position during release. A total force of ~60 kN was applied through the anchor bolts during slot drilling, to ensure proper fracture contact and eliminating displacement during the block release. The normal force, produced by the anchor bolt load yielded a safety factor of approximately 9 opposing the weight of the block, assuming a friction coefficient of 0.5. The slot drilling illustrated in Figure 3-5 proceeded with ∅ 120 mm diameter holes starting from the right side of the block and continuing until the fracture surface on the left side of the block had been reached. The rock bridge on top of the block, marked as the area between the two black arrows, was released last in order to minimise rotation. No rotation was observed from the LVDT sensors. Once slot drilling was completed, the jacks and load cells were connected to a data logger, DataTaker Model DT85, to store data for further analysis. The final test instrumentation is illustrated in Figure 3-4.

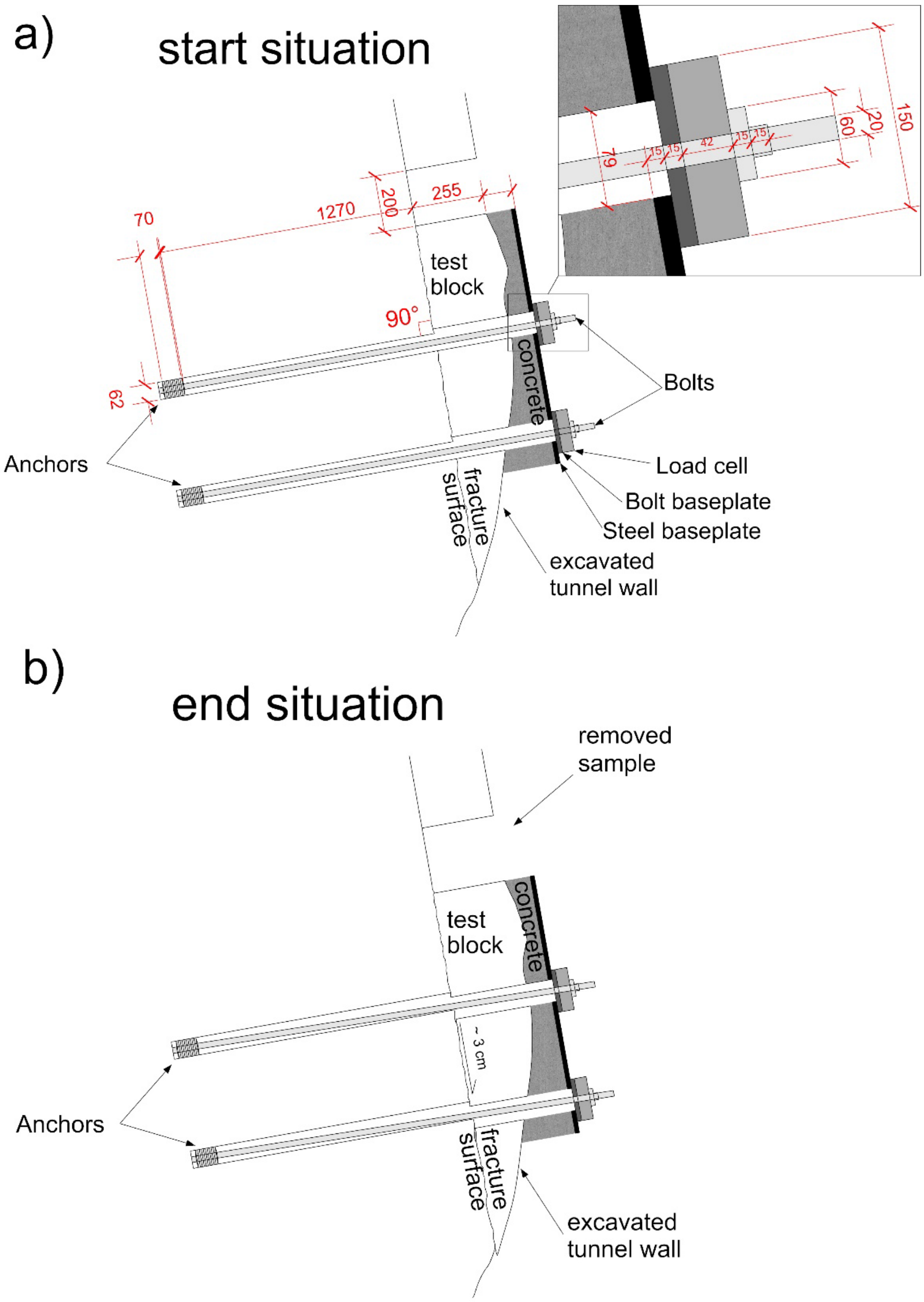

__Figure 3-1.__ Vertical cross-section of the PUSH test setup. a) Initial conditions. b) Post-experiment conditions. Dimensions in millimetres.

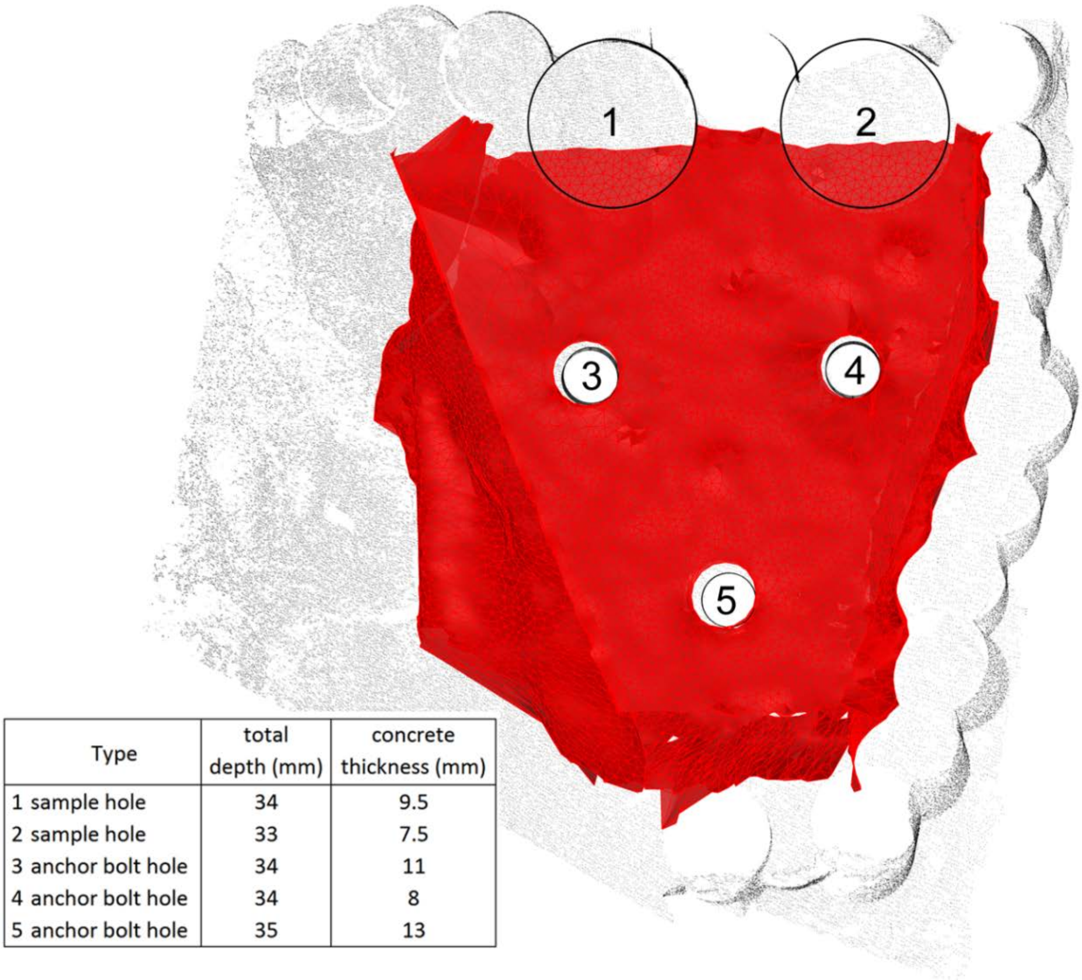

Type	total depth (mm)	concrete thickness (mm)
1 sample hole	34	9.5
2 sample hole	33	7.5
3 anchor bolt hole	34	11
4 anchor bolt hole	34	8
5 anchor bolt hole	35	13

Figure 3-2. *PUSH test layout with measured drillhole depths and concrete thicknesses detailed in an inset table. The test block is illustrated in red.*

Figure 3-3. *Jack baseplates with a jack between them on the left, baseplate dimensions in millimeters on the right.*

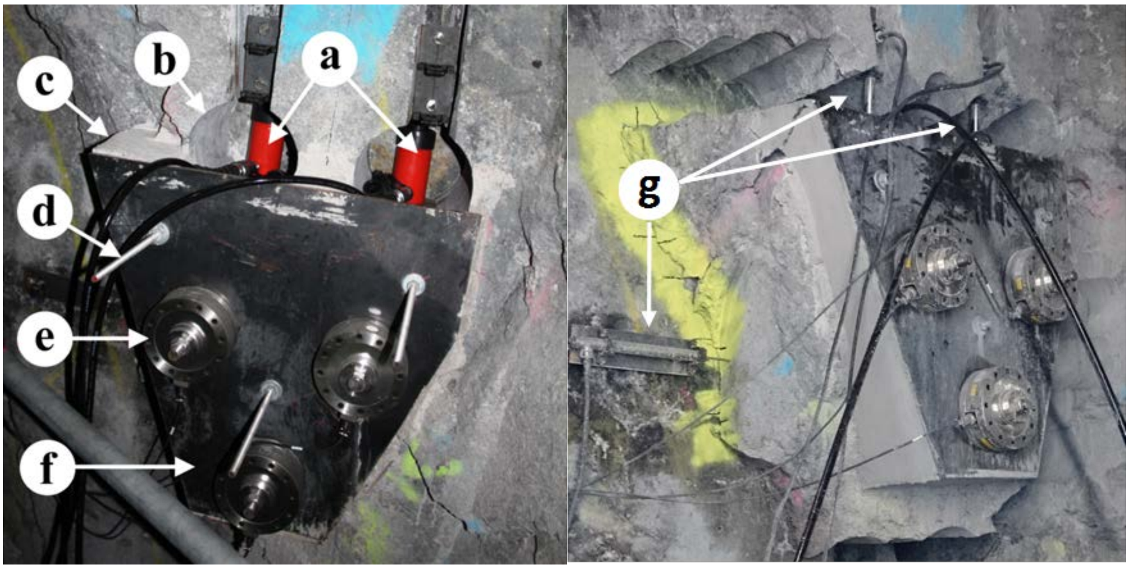

Figure 3-4. *The final instrumentation of the PUSH test. a) jacks, b) removed sample, c) concrete layer, d) attachment bars, e) anchor bolt surrounded by load cell, f) steel slab. The LVDT sensors (g) were installed and connected prior to slot drilling.*

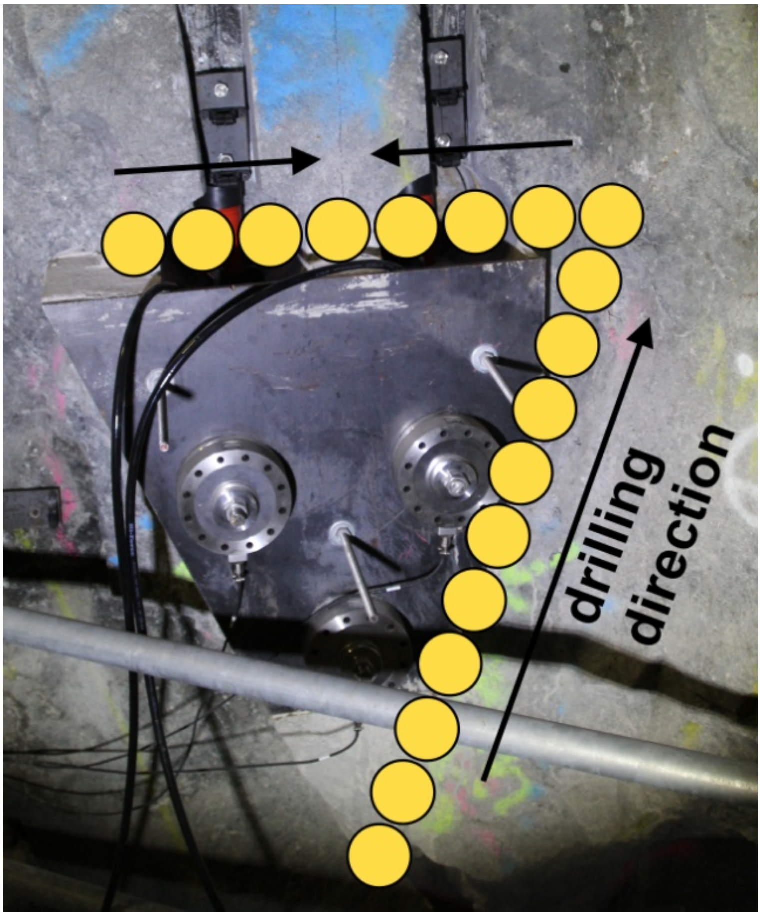

Figure 3-5. *Slot drilling for block detachment. Drilling started from the right side of the block and continued until the fracture surface was reached, painted with a faint pink line on the tunnel wall.*

3.3 Displacement monitoring

The amount of displacement and rotation during shearing of the fracture surface was measured by Linear Variable Differential Transducer (LVDT) sensors. The LVDT sensor is a reliable method for measuring linear displacement and rotation (Hakala et al. 2013). The LVDT sensor converts displacement into a proportional electrical signal. By using phase and amplitude information the direction and the distance of the displacement can then be determined (Wilson 2005). The derived amplitude indicates the amount of displacement and can be converted into millimetres with linear dependence. The LVDT sensor is based on altered output values resulting from the linear movement of a cylindrical ferromagnetic core inside the LVDT sensor, as shown in Figure 3-6 below.

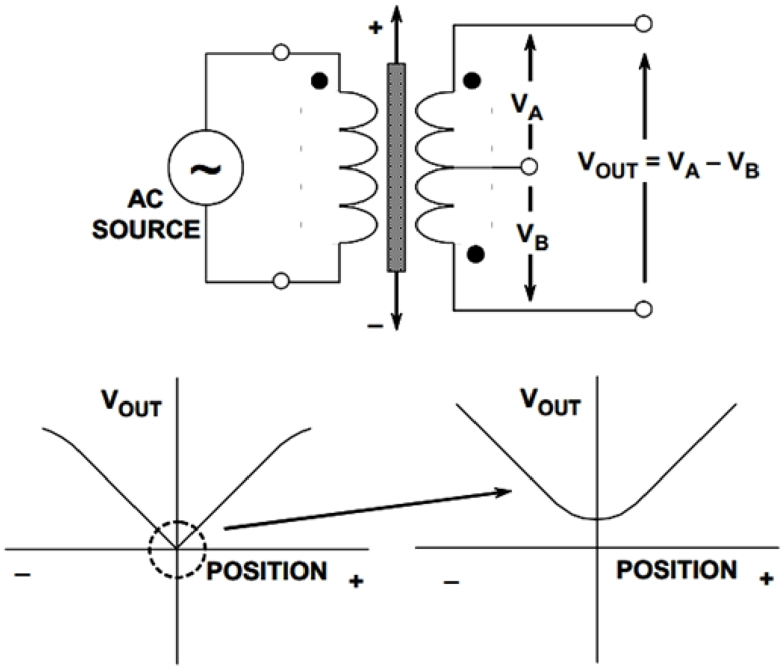

Figure 3-6. *The principle of the LVDT sensor (Wilson 2005). The physical energy of movement is converted into electrical signals as voltage values. The grey bar depicts the cylindrical magnetic core of the LVDT sensor.*

4 PUSH TEST EXECUTION

The experiment began by recording the initial levels of all the monitoring devices. The measured parameters were the output voltage of the LVDT sensors, the shear force produced by the jacks and the normal force produced by the anchor bolts. The initial normal force was set to 20 kN for each individual bolt, based on simulation results detailed in Valli & Hakala, in which it was demonstrated that demonstrated that bolt forces could increase to three times that of the initial value during the planned shear displacement. Further, the maximum load was estimated to be below the maximum LVDT sensor capacity. The initial levels are detailed in Table 4-1.

Two LVDT sensors on the top of the block measured the vertical displacement resulting from shear and one LVDT sensor on the left side of the block measured the rotation that occurred during shear. Normal forces were registered from the load cells and shear forces were registered from the jacks.

Table 4-1. *Initial measurements from instrumentation before the experiment.*

Instrument	Levels before the experiment
LVDT 1 (Left vertical displacement sensor)	45.54 mm
LVDT 2 (Right vertical displacement sensor)	42.33 mm
LVDT 3 (Rotation sensor)	14.77 mm
Hydraulic gauge (Initial pressure on the hydraulic jacks)	5 bar
Load cell (Normal force on each anchor bolt)	20 kN

Prior to beginning final shear to 34 mm, initial shear cycles of 0.2 mm, 0.5 mm and 1 mm were executed to verify equipment performance in order to study shear stiffness and initiation of plastic shear (slip) (Figure 4-1).

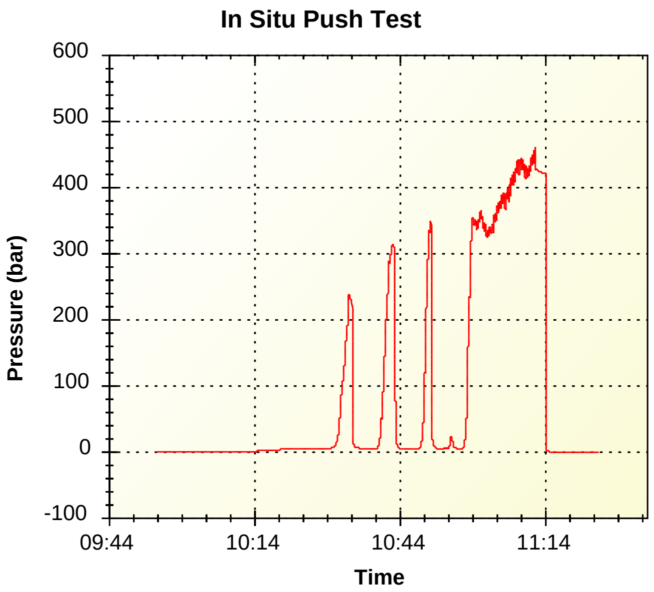

Figure 4-1. *Corresponding 0.2 mm, 0.5 mm and 1 mm shear cycles of the in situ PUSH test of the fractures surface.*

Once the test was complete, the block was weighed and the area of fracture surface behind the block was calculated after releasing it from the tunnel wall. The measured weight of the block was found to be 334 kg and the fracture surface area approximately 0.349 m^2, based on the 3D photogrammetric model (Figure 4-2). The surface area excludes the area of any boreholes. These measurements deviate by +2.7% and -8.5% from the originally estimated values detailed in section 3.2 Note that both the estimated and the measured surface area values excludes parts of the block that broke off during shear, as seen in Figure 4-3 and Figure 4-4. The fracture in the upper left corner does not have any clear indications of being a pre-existing fracture and may have formed as a result of the test (Figure 4-5). The fracture on the right side of the block is clearly a pre-existing fracture due to obvious alteration (Figure 4-6 & Figure 4-7). The larger part of the block that was broken off during shear was estimated to occur between a displacement of ca. 1.8 – 5 mm, based on GoPro video material that captured the execution of the test. When the block was released, the bolts bent back and upon inspection no visible evidence of bolt-rock contact was apparent.

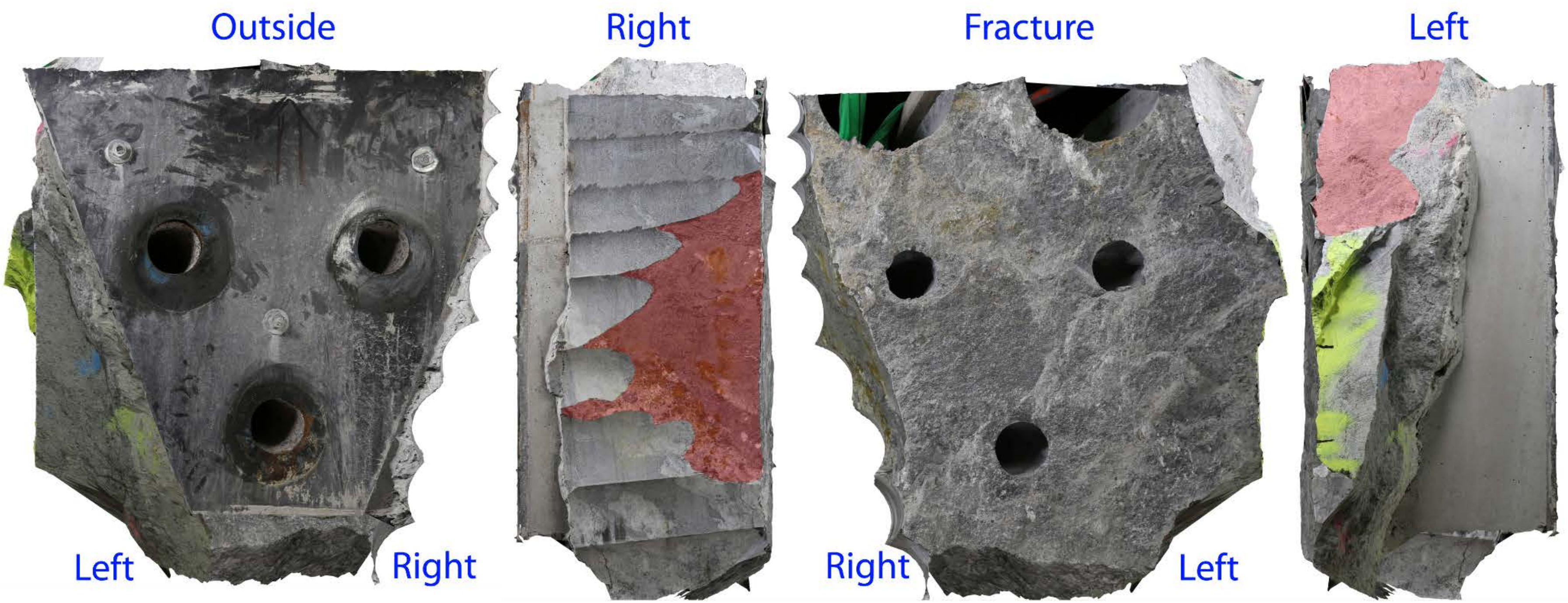

Figure 4-2. *The photogrammetry model of the test block, rotated clockwise from left to right. Areas highlighted in red on the image from the right and left sides of the block indicate pre-existing fractures which caused parts of the block to break.*

Figure 4-3. *Observed breakages after test execution. The upper left corner broke (left) and part of the right edge broke (right). See also Figure 4-3.*

Figure 4-4. *The fracture surface of the block along with the upper left part of the block that broke off during shear, located in the upper right part of the image. Note the smaller part that also broke off the right side of the block, located on the left side of the image.*

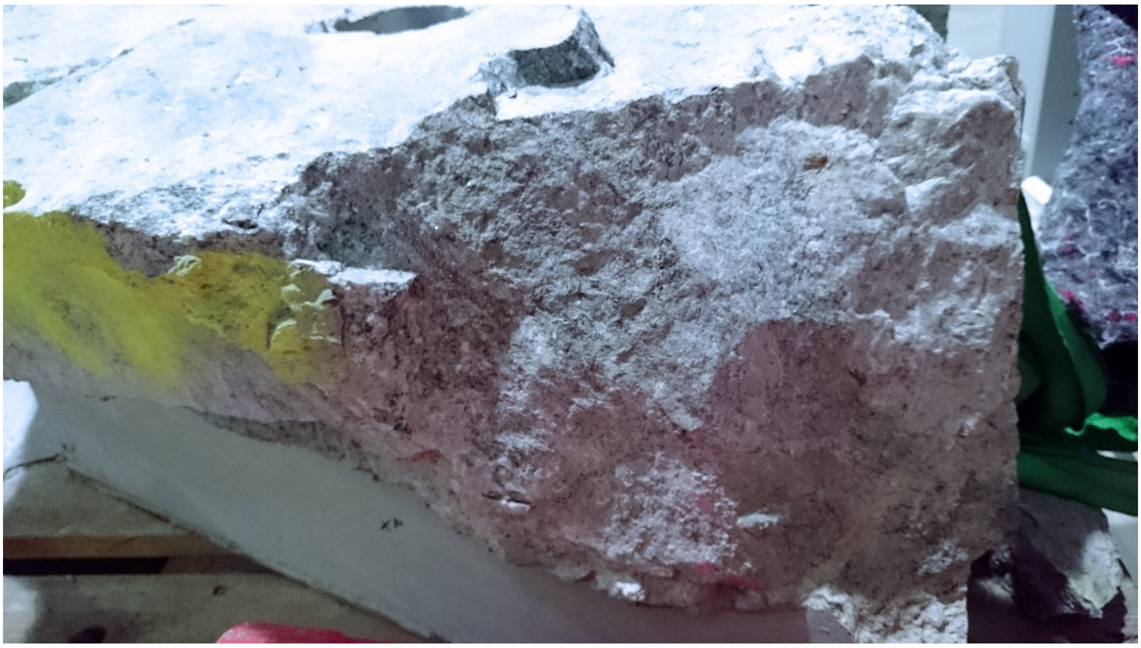

Figure 4-5. *The upper left corner of the block.*

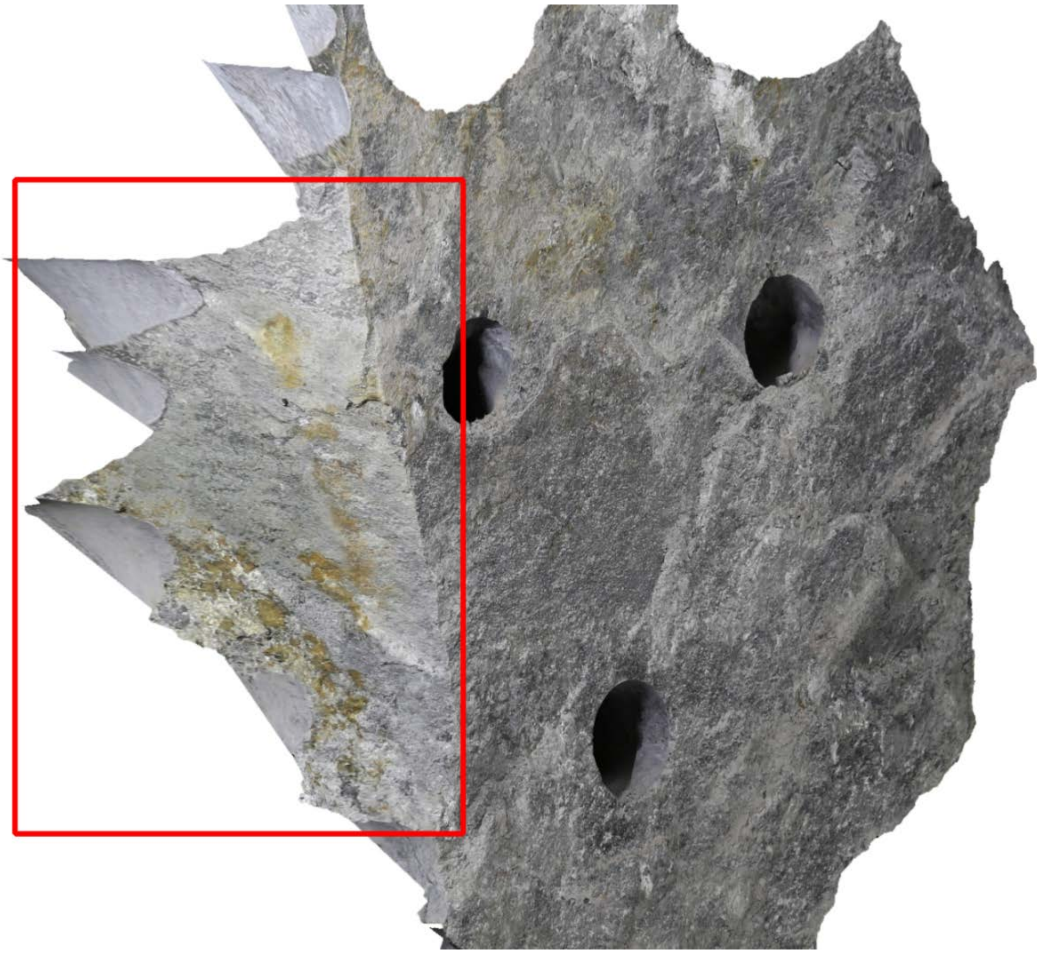

Figure 4-6. *The fracture surface on the right side of the block, viewed from the shear fracture side after block detachment. Note the alteration of the fracture surface, indicating the fracture pre-existed prior to test execution.*

Figure 4-7. *A close-up of the natural fracture surface on the right hand side of the block.*

5 EXPERIMENT RESULTS

5.1 Measurements

A positive displacement of 4.46 mm was registered from the LVDT sensor on the side of the block, whereas the LVDT sensors on top of the block registered displacements of 30.4 mm and 35.95 mm, from the left and right, respectively (Figure 5-1 and Figure 5-2). Bolt forces increased asymmetrically resulting in peak forces of 104 kN, 61 kN and 57 kN for the left, right and bottom bolts, respectively (Figure 5-3). The shear stress estimated based on combined jack forces divided by the estimated fracture surface area (0.319 m^2) (Figure 5-4) reached an initial level of 0.45 MPa and climbed to near 0.6 MPa (Figure 5-5). Similarly the normal stress was evaluated according to the combined bolt forces registered by the load cells divided by the fracture surface area and reached near 0.7 MPa after beginning at a level of 0.2 MPa (Figure 5-5). The estimated window of time for which the test block breaks in the upper left corner was estimated based on GoPro video material, using audio and visual triggers (Figure 5-5). Plotting the shear and normal stress results on a graph that includes theoretical peak shear strength envelopes for JRC's of 6, 12 and 16 obtained from Equation 5-1 (Barton & Choubey 1977) results in an eventual match for a JRC of 6 (Figure 5-6). Finally, the shear strength of the interface between the baseplates and the steel plate was determined empirically using tilt table testing (Figure 5-7). Removal of the outliers values resulted in an average friction angle of 18.1°.

$$\tau = \sigma_n \tan \left[JRC \log_{10}\left(\frac{JCS}{\sigma_n}\right) + \Phi_r \right] \qquad \textit{Equation 5-1}$$

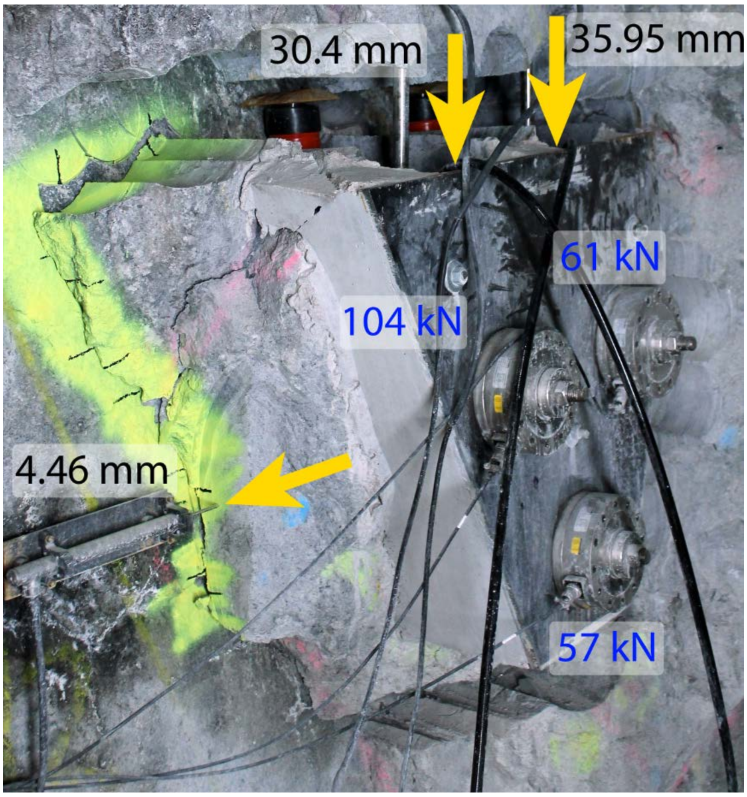

Figure 5-1. *Final position of the test after 30 mm of shear displacement had taken place.*

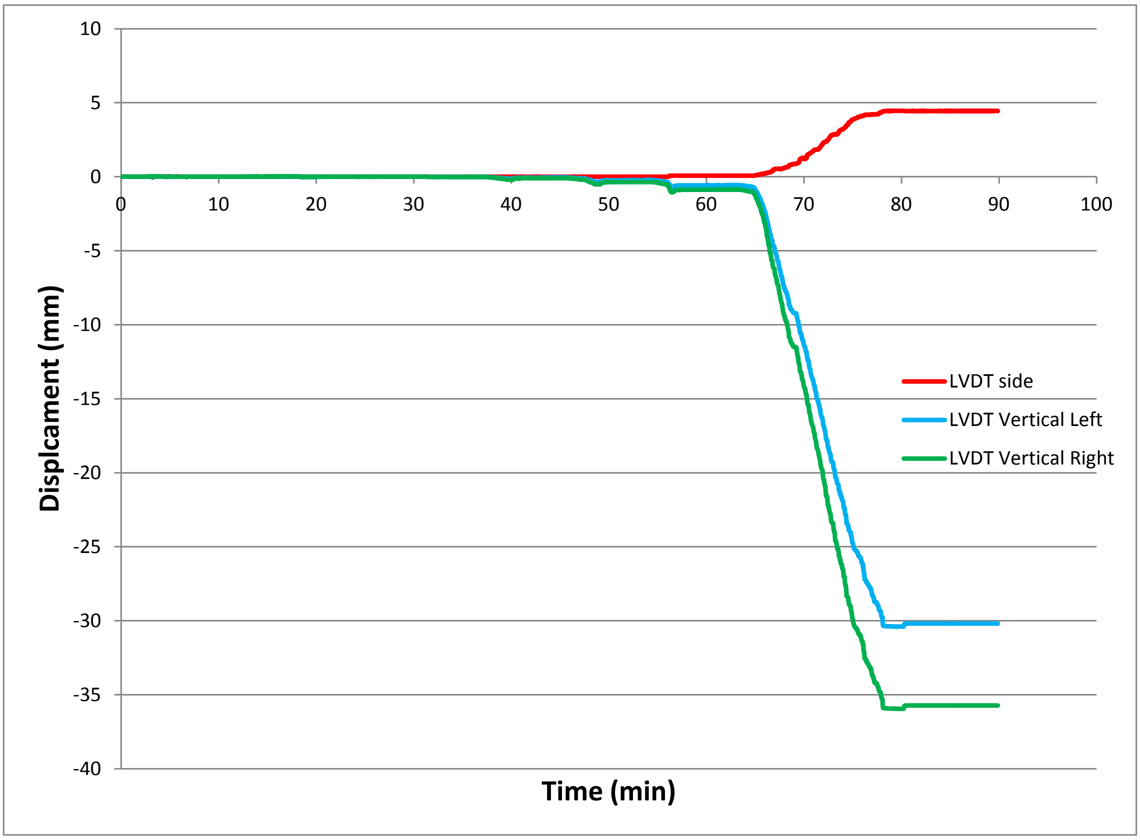

Figure 5-2. *LVDT displacements in mm vs. time in minutes.*

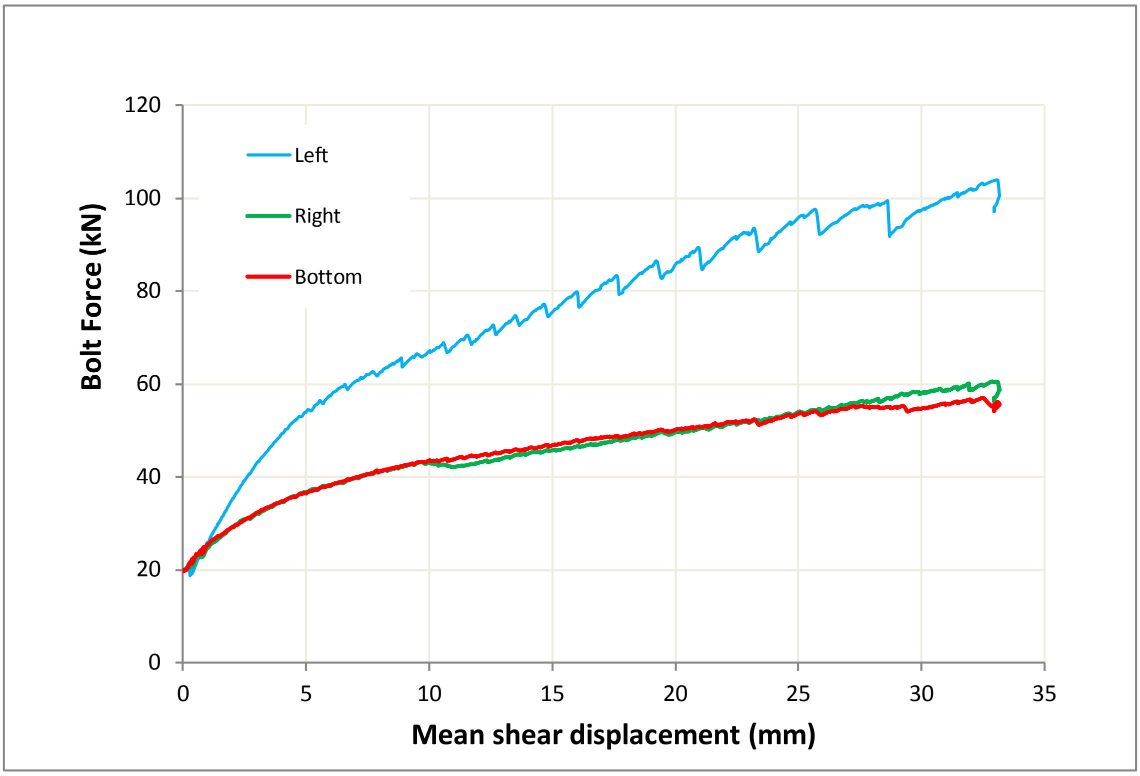

Figure 5-3. *Bolt forces in kN vs. mean shear displacement in mm.*

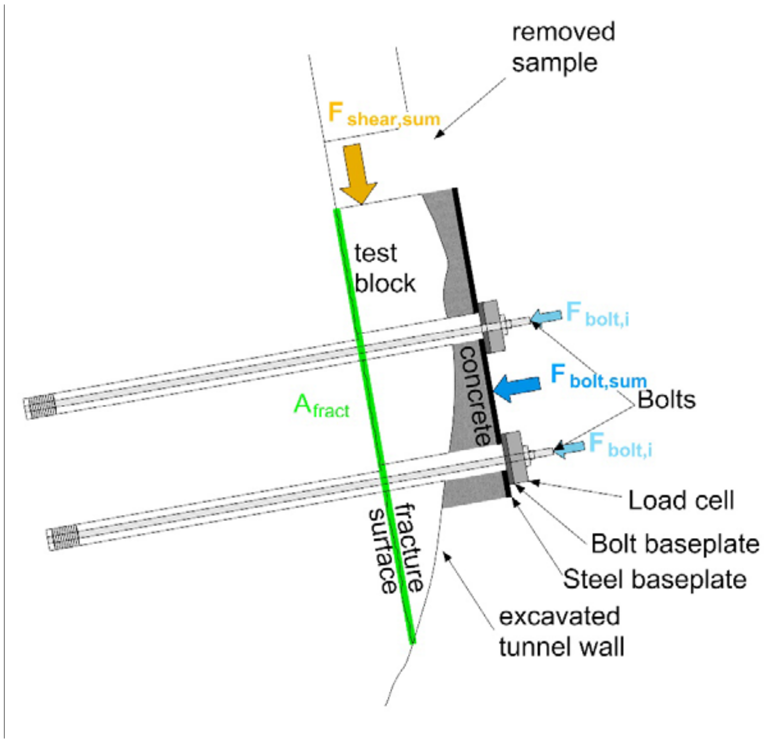

Figure 5-4. *A conceptual image indicating the elements used to determine shear and normal stresses during the experiment. Shear stresses were determined using the summed shear forces from the jacks and the fracture surface area (A_{FRACT}), normal stresses using the summed bolt forces and the fracture surface area.*

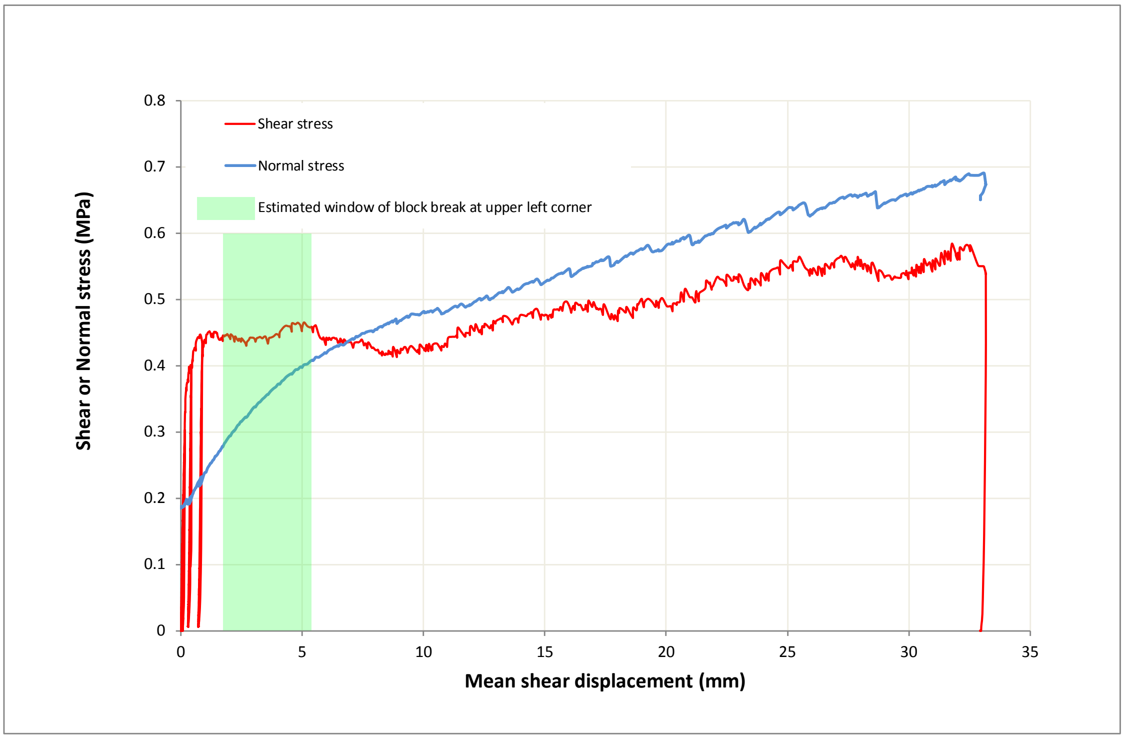

Figure 5-5. *Shear and normal stress in MPa vs. mean shear displacement, based on the estimated fracture surface area (0.319 m^2) and combined jack/bolt forces. The estimated window of time for which the test block develops a fracture in the upper left corner is indicated by a shaded green area.*

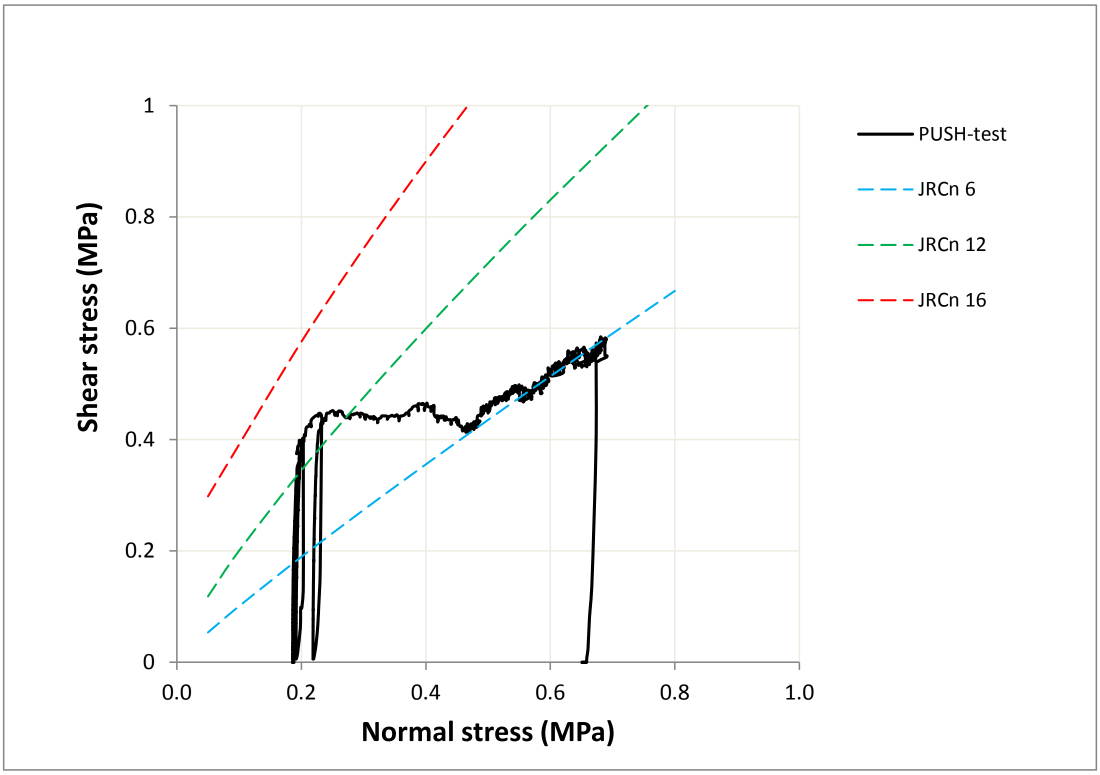

Figure 5-6. *Shear vs normal stress in MPa with envelopes for JRC's of 6, 12 and 16.*

Figure 5-7. *Tilt testing of the bolt faceplate and steel plate interface. Note that tilt testing was performed with extra bolt faceplates on top of the original faceplate and load cell configuration so as to minimise adhesion of the lubricant used between the steel plate and the bolt faceplate.*

5.2 Fracture contact points

The fracture surfaces of the block and wall were mapped after the experiment by a structural geologist to identify fracture contact points (Figure 5-8, Figure 5-9 and Figure 5-10). There was no evidence of intact rock bridges. Areas of the fracture that were open were identified primarily by occurrence of drilling mud. This resulted in an estimated contact area of 3 – 4 % (Figure 5-11). By flipping the block image and scaling it (due to different photography conditions), a fairly good match is found between the mapped contact areas (Figure 5-12). A ridge is apparent on both the fracture surface of the block and the tunnel wall and is ca. 1.5 mm in height (Figure 5-8 and Figure 5-9), although the ridges do not match in geometry. No major damage was apparent at either ridge.

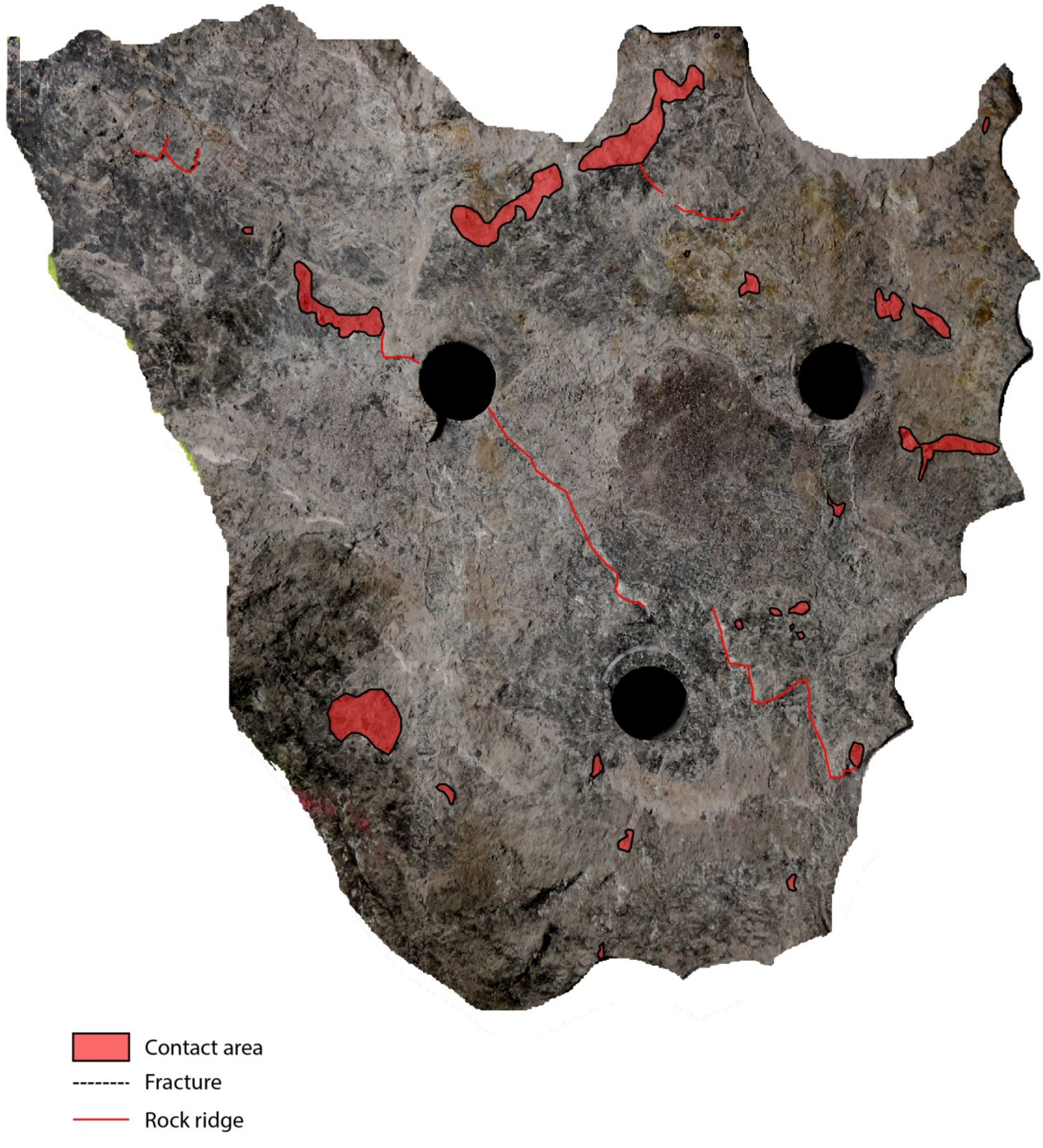

Figure 5-8. *The fracture surface as seen on the tunnel wall. Contact areas of the fracture surface indicated in red. Major rock ridges are marked as red lines.*

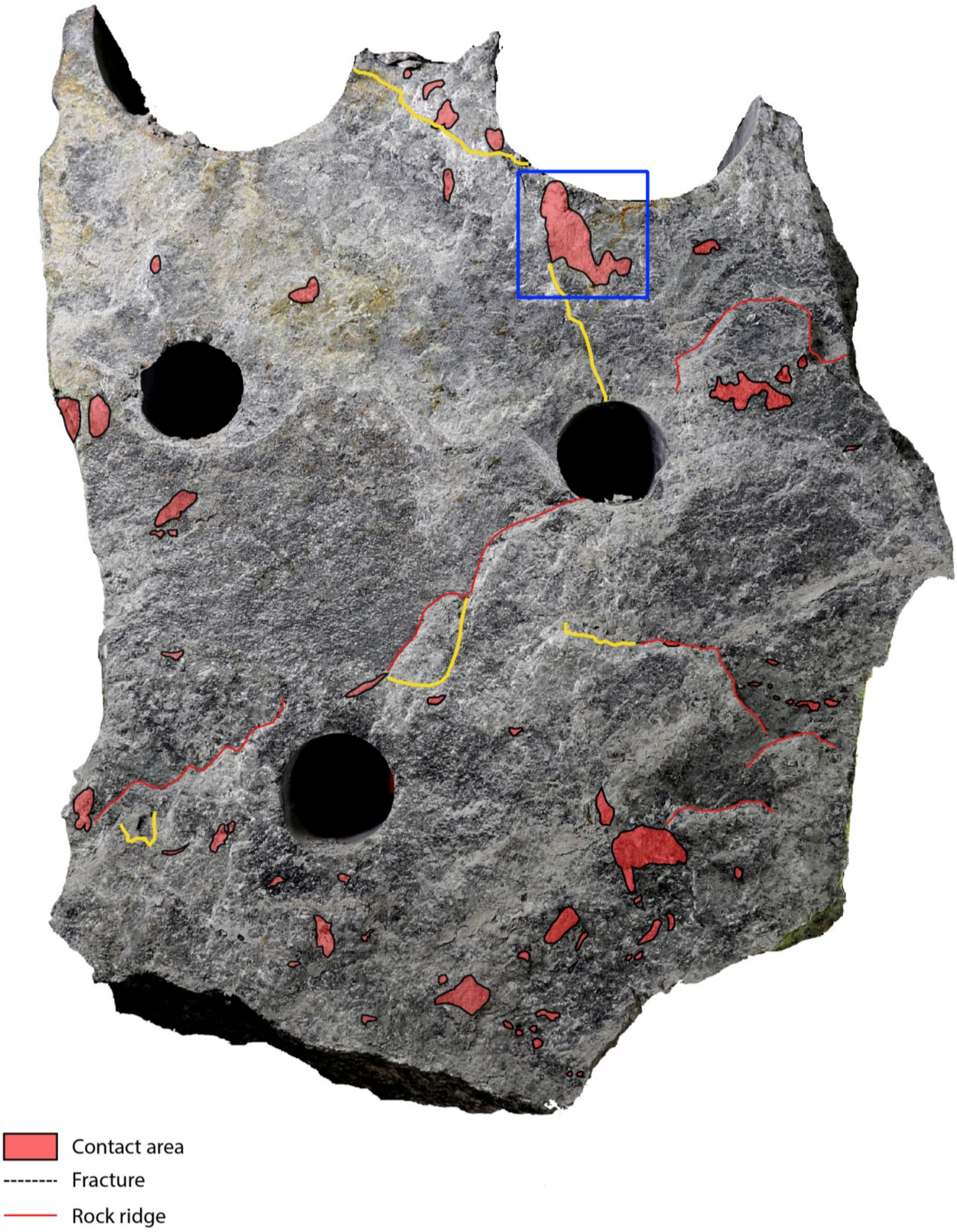

Figure 5-9. *The fracture surface as seen from the block (the bottom left edge and top right are locations where parts of the block are missing). Contact areas of the fracture surface indicated in red. Major rock ridges are marked as red lines and individual fractures in yellow. The border of Figure 5-10 is marked in blue.*

Figure 5-10. *An example of a sheared area that exhibited a clear slickenside surface.*

Figure 5-11. *The open fracture surface area as estimated from the wall, indicated in a beige overlay.*

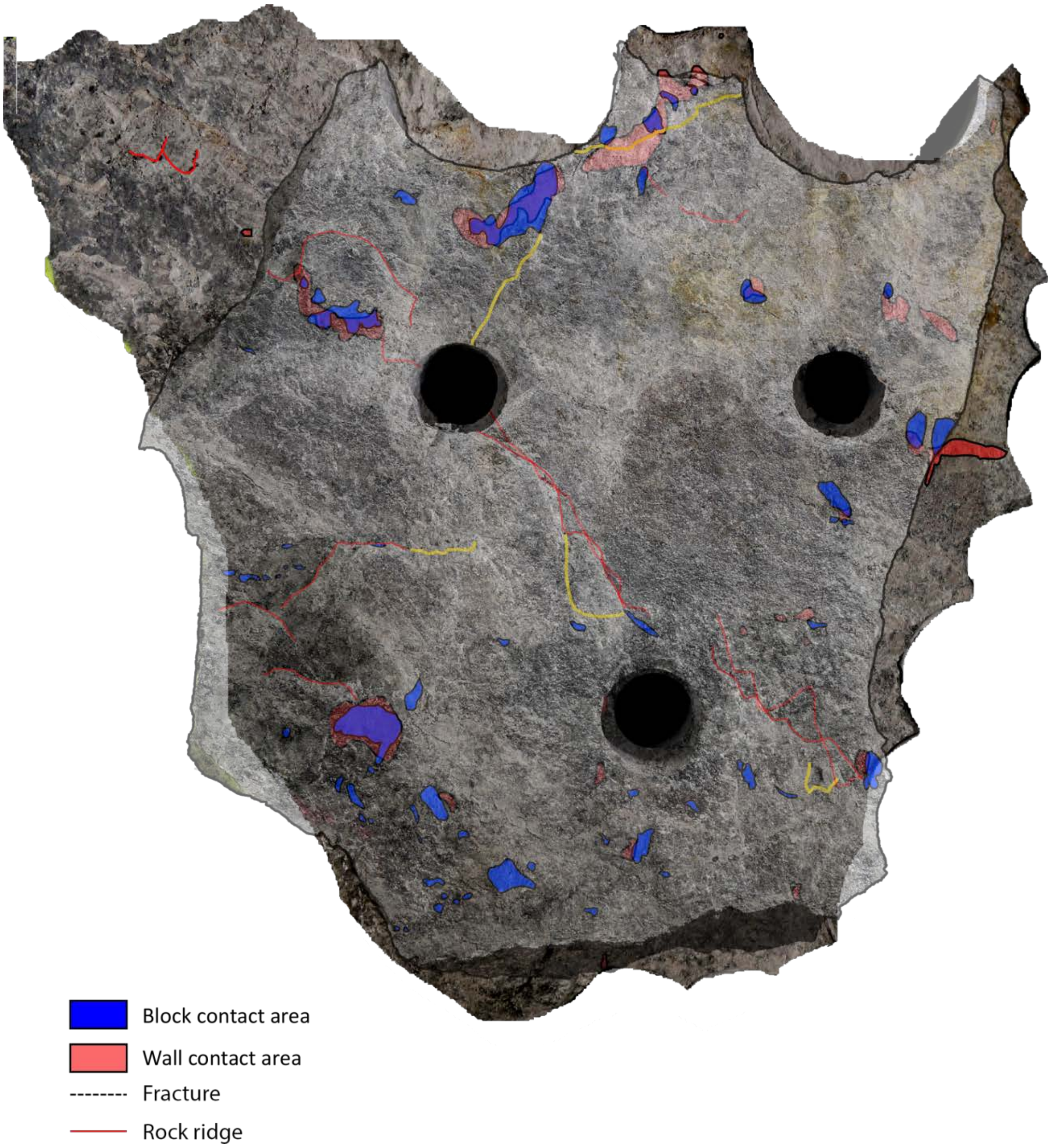

Figure 5-12. *The block contact areas overlaid on top of the wall contact areas by flipping and scaling the block. Blue areas indicate contact areas mapped from the block and red areas mapped from the wall.*

6 BACK-ANALYSIS

6.1 Approach

Back-analysis was performed using 3DEC (Itasca 2015), a three-dimensional computer code that is able to incorporate both a strain-softening rock mass as well as a continuously yielding fracture model. Performing an even remotely accurate back-analysis required positioning the block in its original position (prior to shear) as precisely as possible. Originally this numerical analysis was planned as a prediction-outcome exercise but evolved into back-analysis and thus the original position of the block had not been marked properly on the wall, which resulted in the following procedure for fitting the block in its original position:

1. Block detachment
2. 3D photogrammetry of the block and wall to generate dense point clouds
3. Create best-fit cylinders from the slots drilled into the wall
4. Create opposing best-fit cylinders on the block
5. Orient the block by matching these cylinders as well as possible (Figure 6-1), leaving a small gap prior to "closing" the fracture surface by applying normal stress equal to the pretension force of the constraining bolts.

Once positioned, both the fracture surface on the wall and the block were triangulated to generate 3D surfaces (Figure 6-2). The earlier prediction simulations of the POST - Project published in Valli & Hakala (2016a) had indicated that a densely meshed mated model could be solved within a reasonable time frame, in which the approach consisted of immediately using a densely meshed version of the fracture model with unmated fracture surfaces. This was, however, later abandoned in favour of an approach where the models progressed from simple to more complex (Figure 6-3), as the use of 3DEC to solve a densely meshed unmated version was found to be problematic. In order, the models reported at this time include:

1. A fully planar model
2. A coarsely meshed fully mated model
3. A coarsely meshed unmated model

The planar representation of a fracture was used to test if realistic fracture behaviour could be achieved using solely fracture parameters, instead of incorporating geometry.

A fully-mated model is defined in this report as a single fracture surface with identically matching opposing sides, fully in contact with each other. An unmated fracture surface can be considered to be composed of two independent surfaces that as a result are not fully in contact with each other. The concept of fracture matedness is described in Johansson (2015).

Both the bolts, baseplates (including the thickness of the load transducers) and bolt holes were initially simplified to square geometries with diagonals that matched the original diameters of each respective element (Figure 6-4). Bolt hole diameter, however, later had to be scaled by a factor of 1.35 – 1.5 thereby making them larger in order to avoid contact between the bolts and the rock mass during shearing (Figure 6-5), because the preliminary simulation results indicated that this did not happen in the *in situ* test. The block geometry was also simplified to some degree by defining the edge of the block in a limited number of segments. The modelled rock volume of the wall was limited to a depth of ca 5 cm, but the normal loading bolts were modelled using actual lengths. The effect of these simplifications on the back-analysis was considered negligible.

Finally, the block was brought into contact with the wall using the initial bolt normal forces used in the experiment, whilst allowing for block rotation, thus enabling the block to reach as good of an original position as possible (Figure 6-6 and Figure 6-7). Note that although the block is oriented in the simulation so that shear occurs along the x-axis of the model, gravity has been applied according to the actual orientation of the experiment. Normal stress prior to shear in the fully-mated model is higher on the right side of the block as the bolts are not equally distributed across the fracture surface (Figure 6-6). Fixed boundary conditions were applied to the sides and the bottom of the wall as well as to the ends of the bolts. Once the block had settled, shear was induced by applied uneven constant velocity boundary conditions to the location of the jacks (Figure 6-8). Constant velocities were used in order to back-analyse fracture stiffness and shear strength parameters. Extremely long calculation times would have resulted for all cases where shear strength is higher than *in situ* if the simulations had incorporated measured jacking forces.

Table 6-1. *Simulation phases of forced block shear.*

1	Compressing the surfaces into contact under upper block normal stress equal to bolt pretension force, bolts pretensioned and free to slide through baseplates
2	Locking the bolts to the baseplates
3	Shearing the block up to 35 mm by applying constant velocities at hydraulic jack contact lines. Note that the velocities are uneven based on measured jack forces

It should be noted that during the *in situ* experiment the shear load was removed three times at the beginning of loading in order to study shear stiffness and initiation of plastic shear (slip).

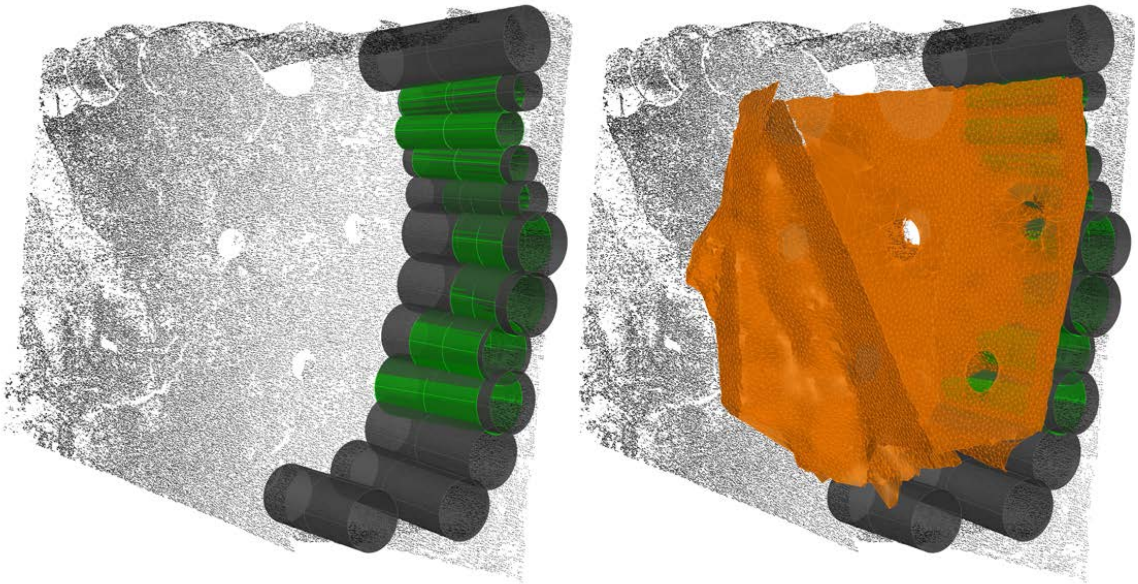

Figure 6-1. *The point cloud of the wall in black, the best-fit cylinders of the wall in dark grey, the opposing block cylinders in green and the block in orange when in place.*

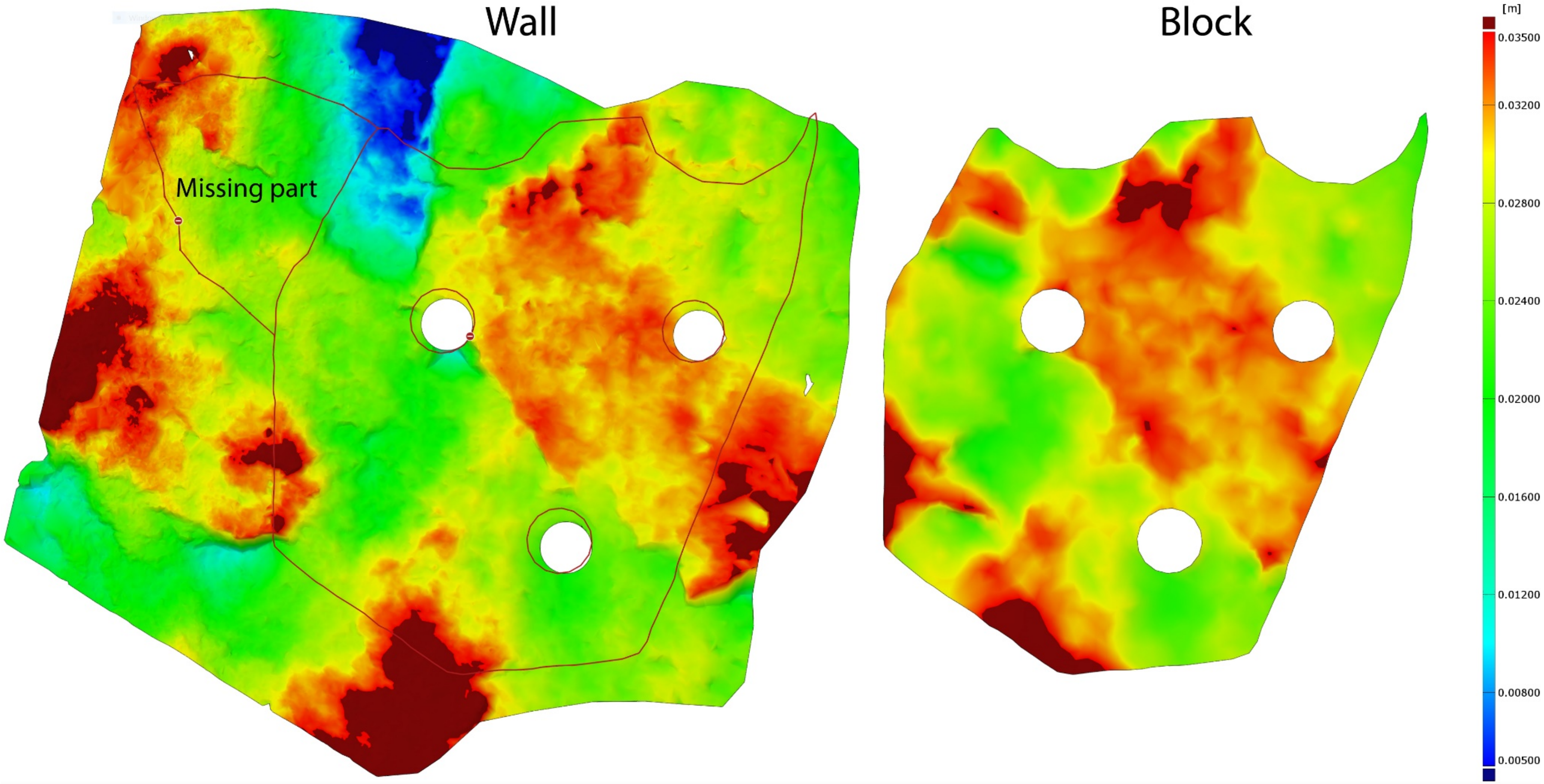

Figure 6-2. *Wall and block topography using the lowest point of the tunnel wall as the frame of reference for both surfaces using a mesh with an edge length of 1- 1.5 cm. The outline of the block is illustrated on top of the wall along with an estimate of the missing part of the block. View perpendicular to the fracture surface.*

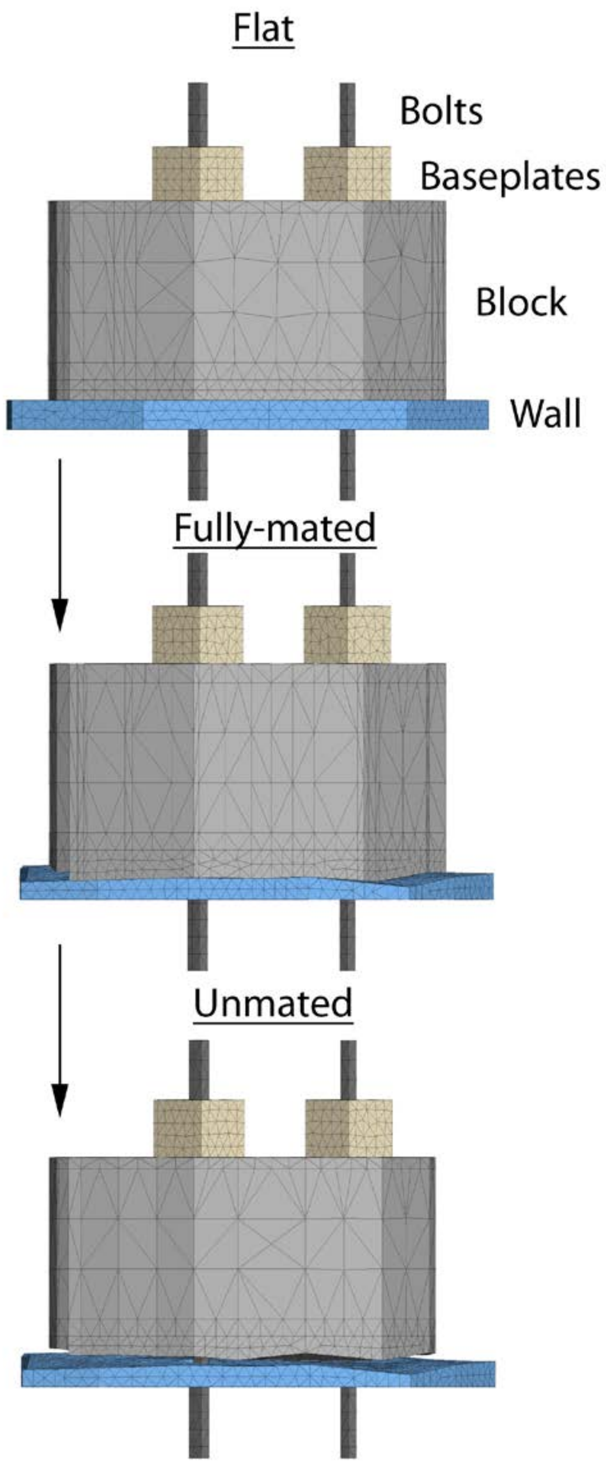

Figure 6-3. *Model progression from flat to fully-mated to unmated. Note that baseplates also include the thickness of load transducers.*

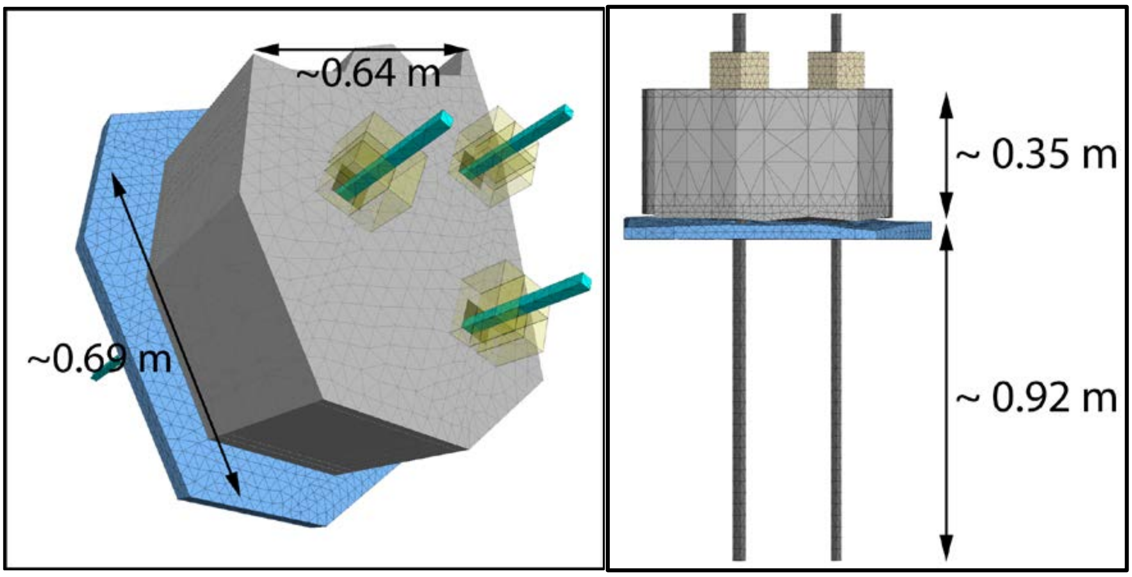

Figure 6-4. *Left: The planar version of the simulation model, with the wall surface in light blue, the block in grey, the bolts in cyan and the baseplates in transparent yellow. Right: a view from the left side of the unmated model. The thickness of the block was matched to the thicknesses measured in the experiment according to hole and bolt lengths.*

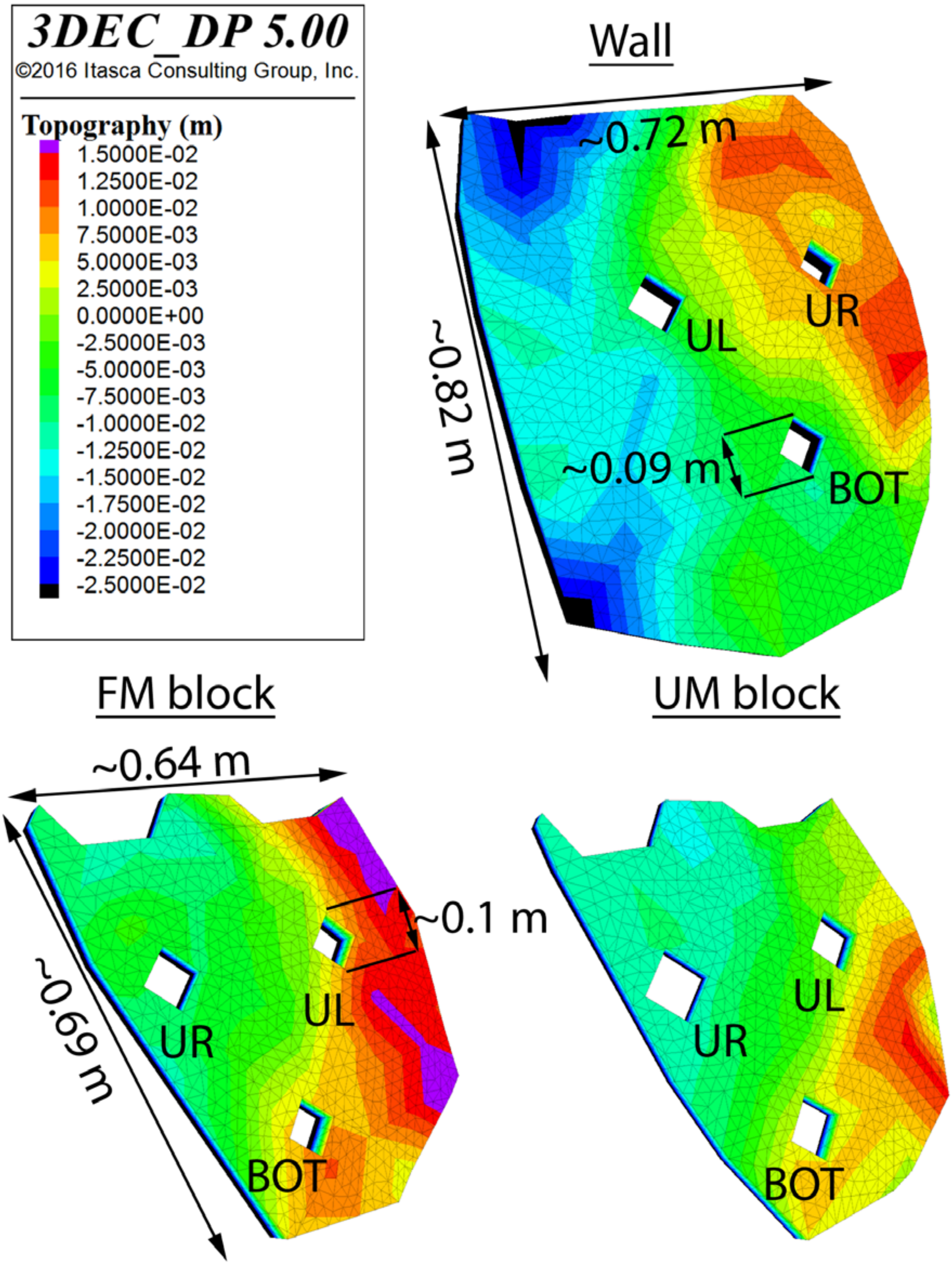

Figure 6-5. *Fracture surfaces coloured according to topography with over 1.5 cm coloured in violet and under – 2.5 cm coloured in black, using the model Z plane at 0 as the frame of reference. Top: the wall of the coarse model version. Bottom from left to right: a mirror image of the block of the coarse fully mated and unmated models, respectively. Note the bolt holes in the block and wall that were simplified to square geometries with scaled diagonal lengths of 0.1 m and 0.09 m, respectively.*

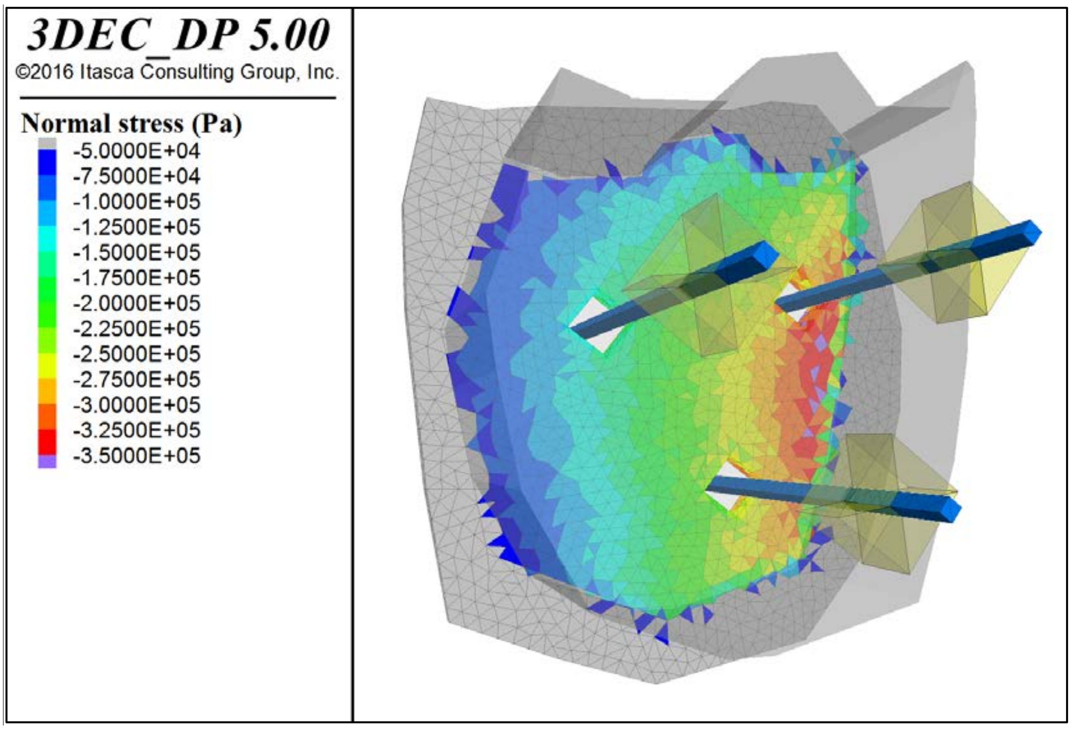

Figure 6-6. *The normal stress from the fracture surface prior to shear from the fully-mated version of the model. Below 50 kPa in grey, over 0.35 MPa in violet.*

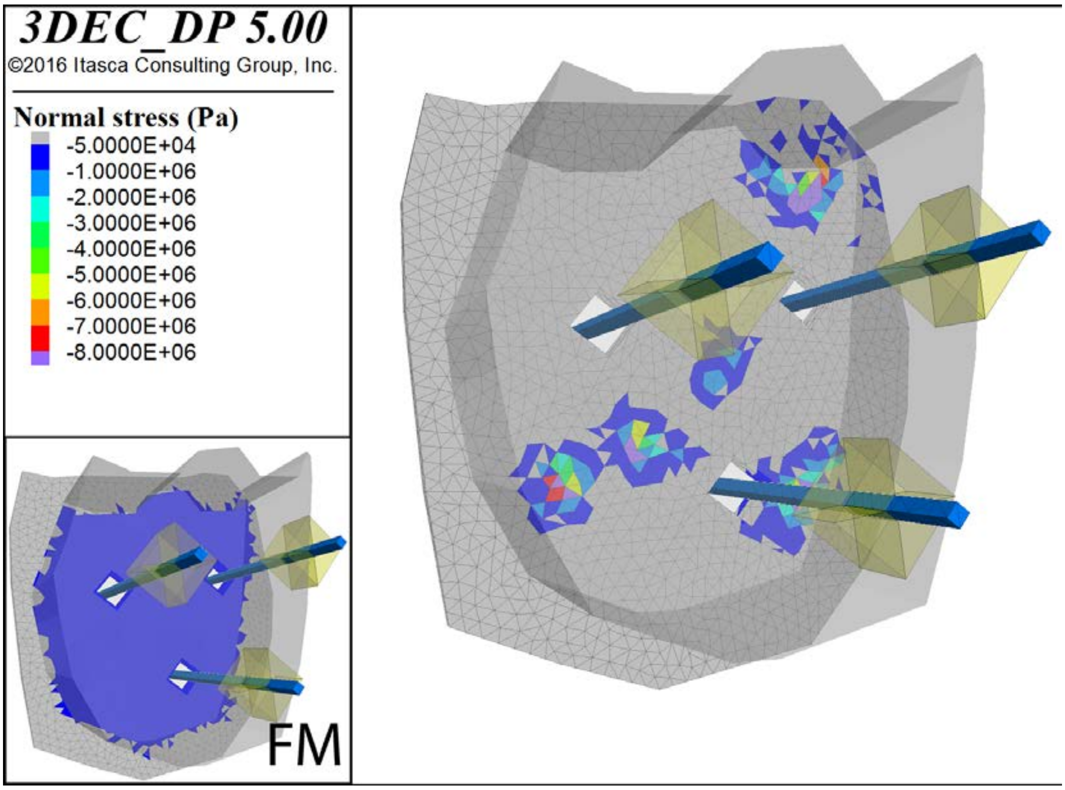

Figure 6-7*. The normal stress from the fracture surface prior to shear from the unmated version of the model. Below 50 kPa in grey, over 8 MPa in violet. Note the different stress scale. An inset of the fully-mated model using this stress scale is illustrated in the bottom left corner.*

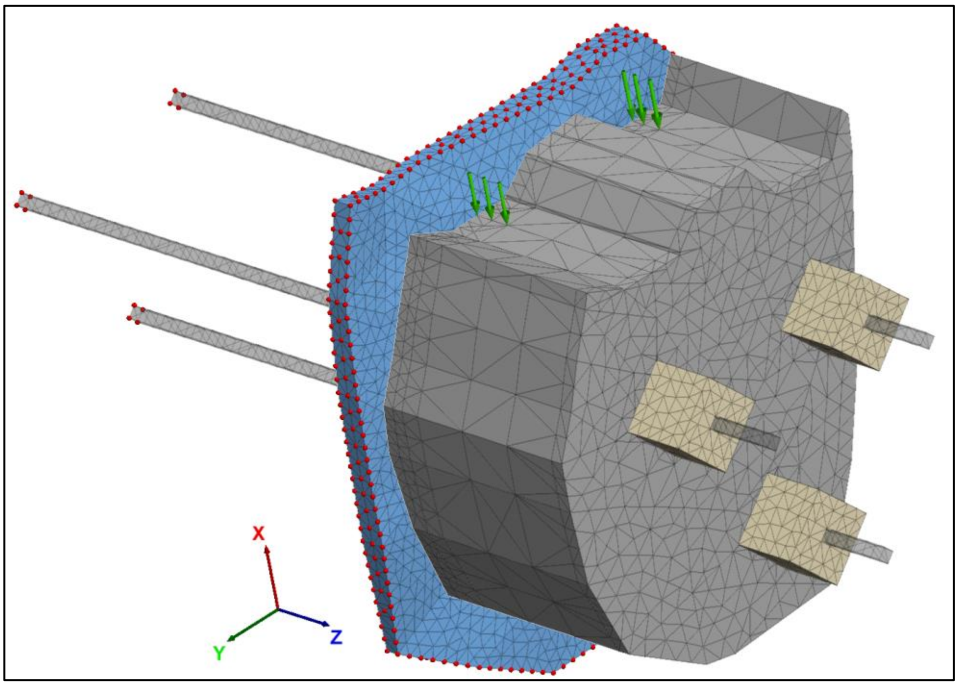

Figure 6-8. *The boundary conditions during shear. Red spheres indicated fixed locations and green arrows indicated applied constant velocity boundary conditions. Model axes are not to be confused with the true orientation of the experiment.*

6.2 Parameters

<u>Rock mass</u>

Initial calibrations with the coarse mesh models were performed using an elastic rock mass, with a Young's modulus of 55 GPa and a Poisson's ratio of 0.2.

The initial rock mass parameters of the block and wall were derived from the average laboratory test crack initiation (CI), uniaxial compressive strength (UCS) and tensile strength (T) results available for Olkiluoto veined gneiss (VGN) from the Posiva 2011 Site Description report (Posiva 2013) using a brittle failure strength estimate, more specifically a cohesion-softening / friction hardening (CSFH) estimate (Diederichs et al. 2010). The high cohesion failure initiation is defined by Crack Initiation (CI) and the extent of damage is limited by the frictional spalling limit. The CSFH parameter values using the Hoek-Brown formulation are defined by the method defined in Diederichs et al. (2010):

$s_{CI} = (CI/UCS)^{(1/a)}$, *and* $a=0.25$

$m_{CI} = s_{CI}\ (UCS/|T|)$

Spalling Limit is obtained by setting a=0.75, s=0 and m=7-10, here m=7 is used

These Hoek-Brown strength envelopes were then replaced with Mohr-Coulomb strain softening/hardening envelopes for use in 3DEC. The secant fitting is done for a σ_3 range of 0 MPa to 7 MPa. The transition from the damage initiation envelope to the spalling limit is assumed to take place linearly during the first 0.005 plastic shear strain for the friction angle. The transition point varies for cohesion (0.0025), tensile strength (0.0001) and dilation (0.0002/0.005). Tensile strength is therefore lost nearly instantaneously at failure initiation and dilation reaches 20° initially after which it is set to 0 once strain has progressed to 0.01 (Figure 6-9). As implied by the CSFH approach, the initial rock mass cohesion is 19.1 MPa and drops to 1.9 MPa whilst the initial rock mass friction is 17° and hardens to a residual value of 50°.

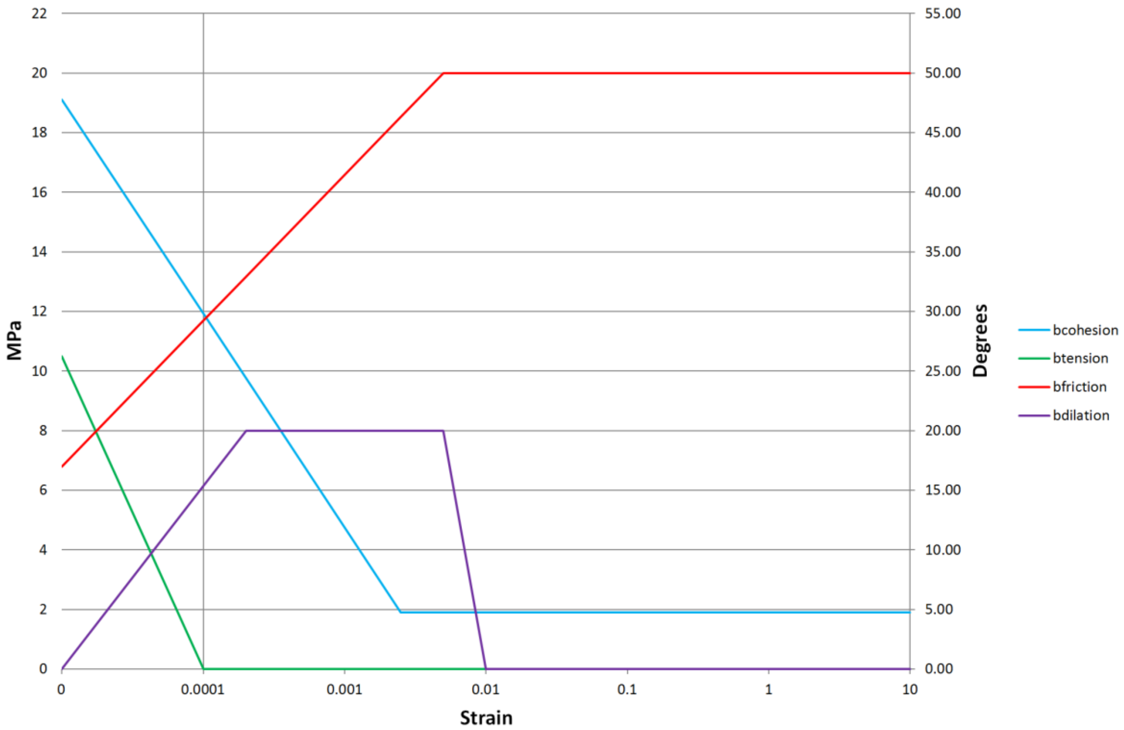

Figure 6-9. *The initial and residual failure envelopes for veined gneiss using a CSFH approach and a Hoek-Brown where D=0 approach. Cohesion in blue, tensile strength in green, friction in red and dilation in violet.*

<u>*Fracture*</u>

Fracture parameters were likewise obtained from the laboratory shear test results available at the time for ONKALO fractures (Jacobsson 2016). A fracture surface from hole ONK-SH81 was selected to be representative of a “soft” fracture surface and therefore its results were used to calibrate shear and normal stiffness models.

Although calibrations using the coarse mesh models were performed both with an elastic/plastic constant stiffness model with Coulomb slip criteria and the continuously yielding (CY) joint behaviour model, the majority of the models were run with the CY model.

The continuously yielding joint model available in 3DEC was selected for use in the simulations as the initial calibrations indicated it resulted in a fairly realistic shear and normal response (Valli & Hakala 2016a). This nonlinear behaviour model is intended to simulate the internal mechanism of progressive damage of joints/fractures under shear in a simple fashion (Itasca 2015). This includes the following:

- The curve of shear stress/shear displacement is always tending toward a “target” shear strength for the joint (i.e., the instantaneous gradient of the curve depends directly on the difference between strength and stress)
- The target shear strength decreases continuously as a function of accumulated plastic displacement (a measure of damage)
- Dilation angle is taken as the difference between the apparent friction angle (determined by the current shear stress and normal stress) and the residual friction angle

As a result the normal and shear stiffness used in the behaviour model can behave as a function of the current normal or shear stress at any given time. The fracture parameters used in the final unmated back analysis were a result of initial calibrations performed to enable as good a match as possible regarding the shear and normal stresses calculated from the data obtained from the experiment.

Calibrations with the planar surface model were performed with the following parameters, of which only the initial friction angle, the residual friction angle and the joint roughness were varied:

- Normal stiffness: 5.1e-5 $\sigma_N^{1.014}$ MPa/mm (within 175 and 10 000 MPa/mm)
- Shear stiffness: 7e-6 $\sigma_N^{1.2}$ MPa/mm (within 10 and 10 000 MPa/mm)
- Initial friction: 45° - 48°
- Residual friction: 38° - 41°
- Joint roughness (CY): 4 – 5.5 mm

Fully-mated surface calibrations with both the Coulomb slip and with the CY joint behaviour model involved the following variation:

- Normal stiffness: 5.1e-6 $\sigma_N^{1.014}$ MPa/mm (CY) - 175 MPa/mm (Coulomb) (within 1 and 10 000 MPa/mm)
- Shear stiffness: 7e-6 $\sigma_N^{1.2}$ MPa/mm (CY) – 10 MPa/mm (Coulomb) (within 10 and 10 000 MPa/mm)
- Initial friction: 30° - 50°
- Residual friction: 10° - 41°
- Joint roughness (CY): 2 – 5.5 mm

Unmated surface calibrations were performed by varying the following CY parameters:

- Normal stiffness: 5.1e-7 $\sigma_N^{1.014}$ MPa/mm - 5.1e-5 $\sigma_N^{1.014}$ MPa/mm (within 175 and 10 000 MPa/mm)
- Shear stiffness: 7e-6 $\sigma_N^{1.2}$ MPa/mm - 14e-6 $\sigma_N^{1.2}$ MPa/mm (within 10 and 10 000 MPa/mm)
- Initial friction: 45° - 50°
- Residual friction: 38° - 42°
- Joint roughness (CY): 5 – 8 mm

6.3 Results

The key results of planar, mated and unmated fracture surface simulations are presented in the form of normal and shear stress for the block. Measured values are calculated from monitored jack forces and bolt forces divided by the fracture surface area (0.319 m^2), as described in section 5.1. Corresponding values are calculated for the model, but in addition the mean normal- and shear stresses are monitored from the modelled fracture, which was naturally not possible in the actual PUSH test. The assumption was that the two normal forces are very close to each other, but significant differences are expected in shear forces for non-planar fracture surfaces (Figures 6-9 to 6-19).

Planar fracture surface

Although unrealistic, the planar representation of the fracture surface could be calibrated to produce a fairly realistic jacking force and bolt load response i.e. the apparent shear and normal stress behaviour. The shear stress levels were lower than observed up to a shear displacement of 8 mm, although normal stress levels were reasonable. After this point shear and normal stress levels were in a sufficiently accurate range (Figure 6-10). The initial shear stress peaks observed during the experiment are most likely a result of the section of the block that broke off from the upper left corner or possibly from geometry i.e. local peaks in topography. An optimum match was reached using the following CY-parameters:

- Normal stiffness: 5.1e-5 $\sigma_N^{1.014}$ MPa/mm (within 175 and 10 000 MPa/mm)
- Shear stiffness: 7e-6 $\sigma_N^{1.2}$ MPa/mm (within 10 and 10 000 MPa/mm)
- Initial friction angle: 48°
- Residual friction angle 41°
- Joint roughness 5 mm

Note that the CY-model calculates the mobilized dilation angle as the difference between the mobilized friction angle and the residual angle, so that dilation is initially equal to the difference between these angles and reduces to zero with shear displacement relative to the given joint roughness parameter R.

Individual bolt forces differed from experiment observations which was expected as this model lacked a geometrical effect (Figure 6-11), with the sum of the bolt forces matching the sum of the forces recorded during the experiment.

Fully-mated coarse fracture surface

The fully-mated coarse version of the model produced an optimum match to experiment results with the following parameters (Figure 6-12):

- Normal stiffness 1 MPa/mm
- Shear stiffness 10 MPa/mm
- Initial friction angle: 50°
- Residual friction angle 38°
- Joint roughness 5.5 mm

Note that the dilation caused by fully-mated surfaces had to be compensated for by low normal stiffness. A lower initial friction angle and higher normal stiffness would have produced the same type of response. Regardless, this unrealistic fully mated model was run as an intermediate phase prior to the realistic unmated model in order to verify model functionality. Individual bolt forces were in better agreement with experiment results than with the planar model, with the upper left bolt deviating by ca. 15% nearer the end of shear (Figure 6-13).

Unmated coarse fracture surface

Finally, the coarse unmated version of the model was found to produce an acceptable match to experiment results using the following parameters:

- Normal stiffness: 5.1e-5 $\sigma_N^{1.014}$ MPa/mm (bounds 175 MPa/mm - 10 000 MPa/mm)
- Shear stiffness: 7e-5 $\sigma_N^{1.2}$ MPa/mm (bounds 10 MPa/mm - 10 000 MPa/mm)
- Initial friction: 47°
- Residual friction: 40°
- Joint roughness: 5 mm

The coarse unmated model is unable to fully match the initial behaviour observed in the experiment and with a varying discrepancy of ca. 4 – 12% after ca. 8 mm of shear (Figure 6-14). Normal stress also deviates by ca. 5 – 10%, although this is more pronounced after ca. 25 mm of shear.

The sum of the bolt forces are similarly in agreement with the experiment (Figure 6-16), although the upper right bolt exhibits a slightly higher force than in the fully-mated model (Figure 6-15).

Shear vs. normal stresses from the simulation match the theoretical peak shear strength envelope of a JRC of 6 similar to the measured response after 5 mm of shear displacement (Figure 6-17). This is close to the degraded JRC_{100} described in Section 2.1. During shear, the fracture surface is in contact at three more extensive and in two to three smaller areas (Figure 6-18 to Figure 6-20). Comparison of σ_1, σ_{zz} and σ_{xx} plots clearly indicate that there is a significant topography induced horizontal stress component close to the surface. Only minor areas exhibit plastic shear strain, which is probably a limitation of the coarse mesh size used when generating the topography (Figure 6-21).

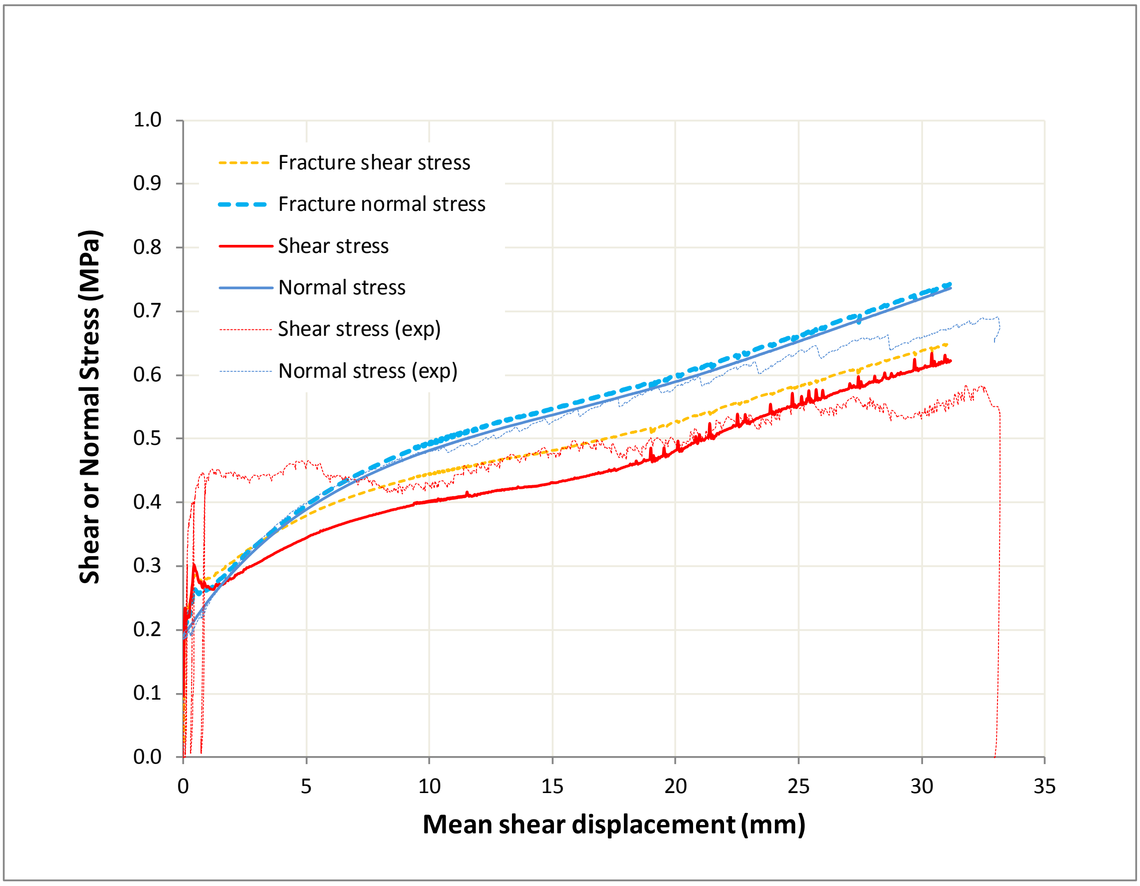

Figure 6-10. *Results from the planar model using an elastic rock mass. Shear and normal stresses registered from the fracture surface indicated as dashed lines. Experiment results as thin dotted lines.*

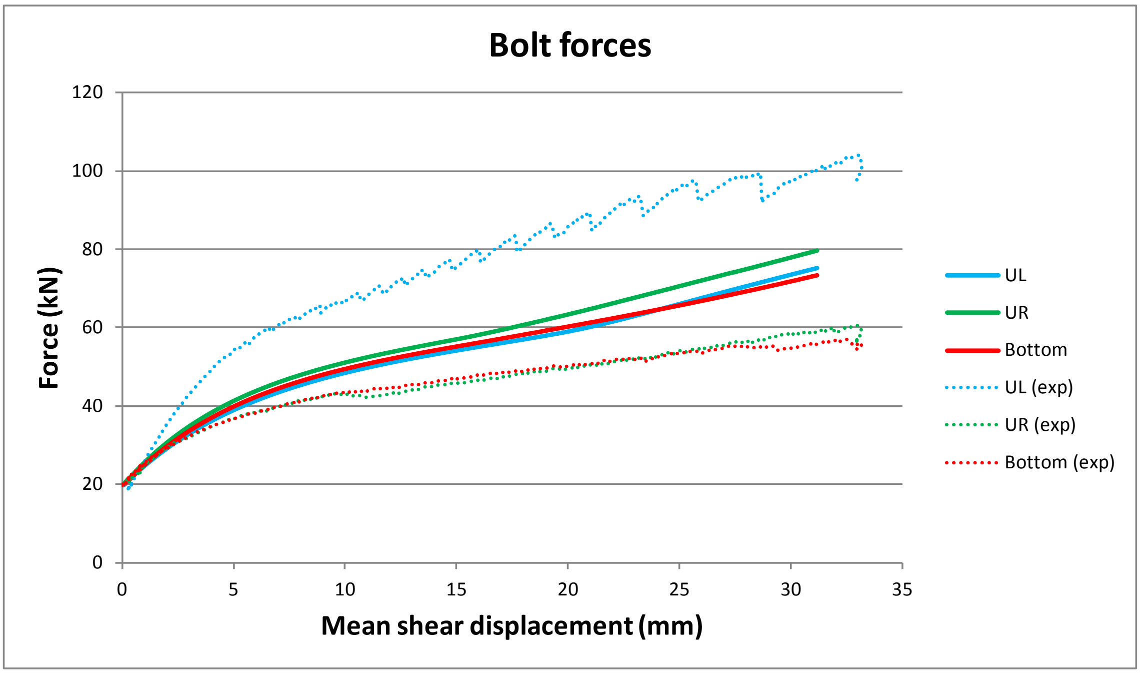

Figure 6-11. *Planar model, elastic rock: Bolt forces in kN, with experiment results indicated as dotted lines. UL = upper left, UR = upper right.*

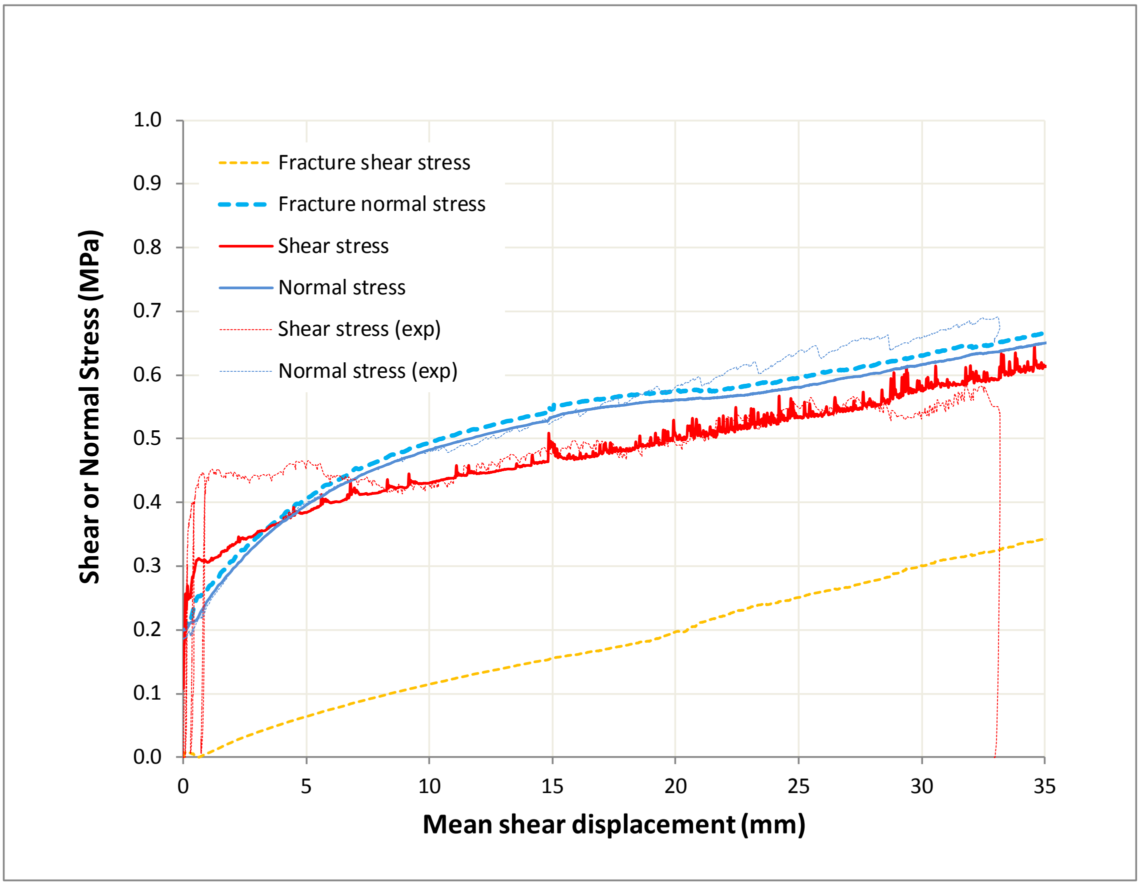

Figure 6-12. *Results from the fully-mated model using an elastic rock mass. Shear and normal stresses registered from the fracture surface indicated as dashed lines. Experiment results as thin dotted lines.*

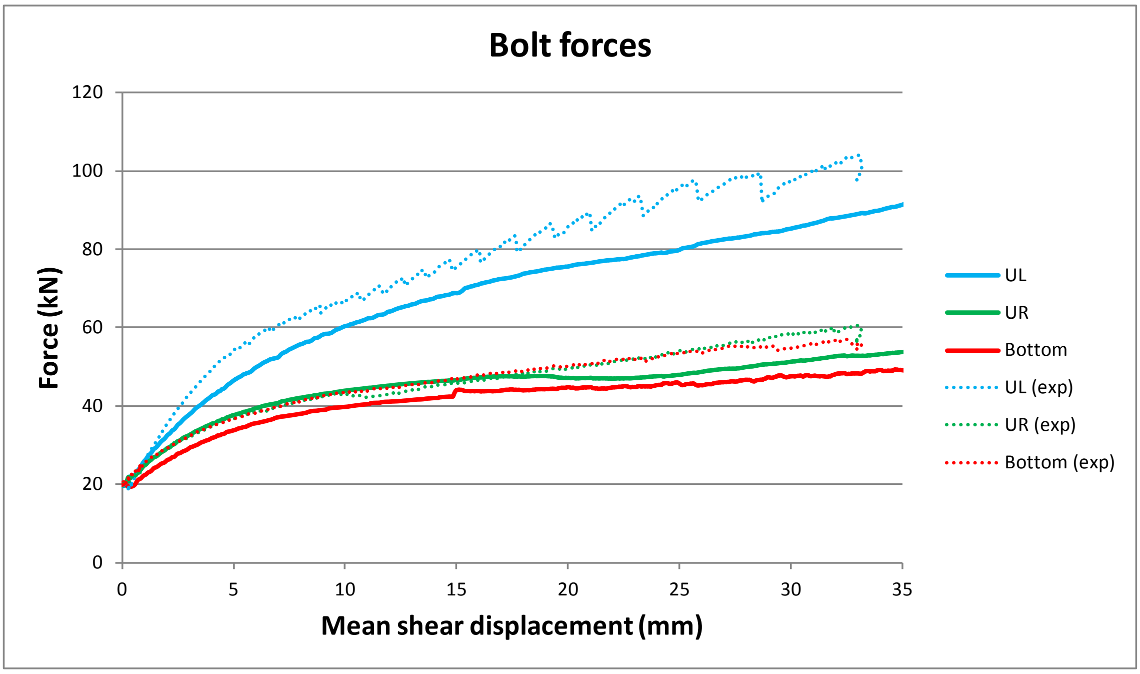

Figure 6-13. *Fully-mated model, elastic rock: Bolt forces in kN, with experiment results indicated as dotted lines. UL = upper left, UR = upper right.*

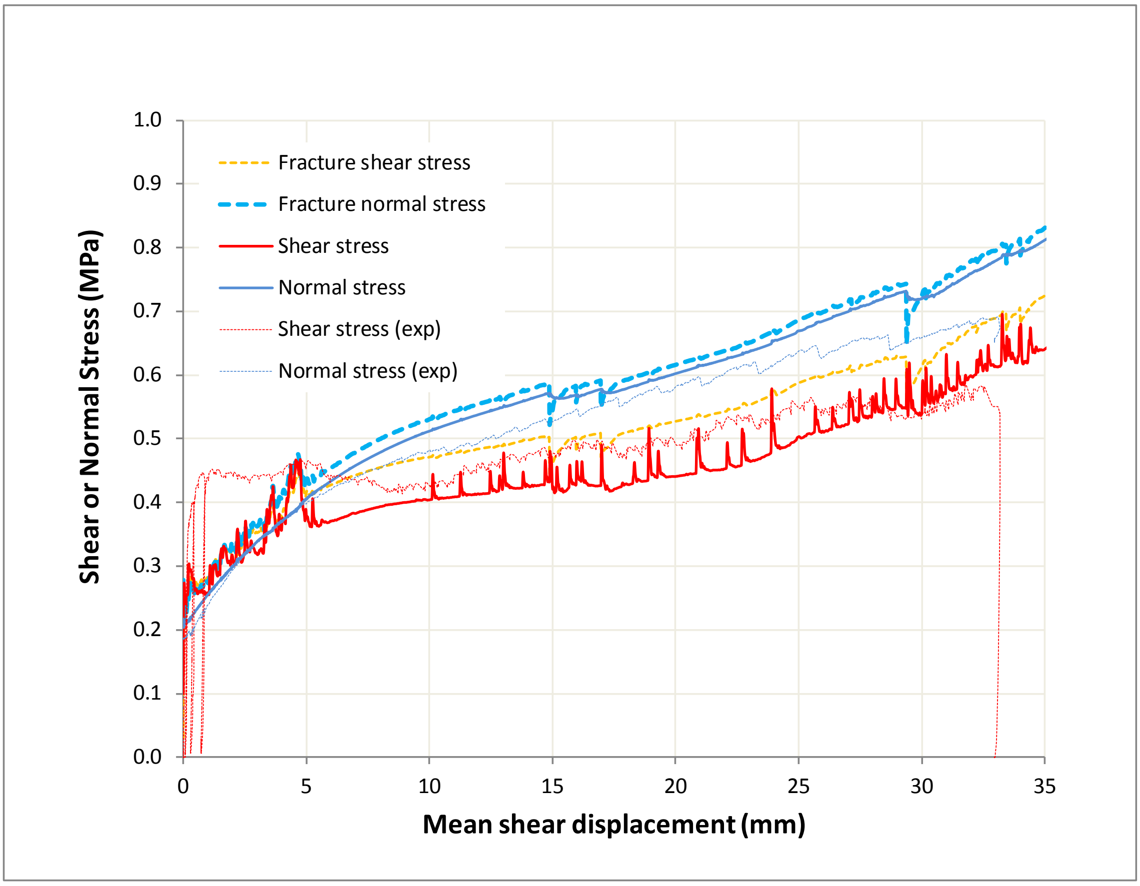

Figure 6-14. *Results from the unmated model using a strain softening rock mass. Shear and normal stresses registered from the fracture surface indicated as dashed lines. Experiment results as thin dotted lines.*

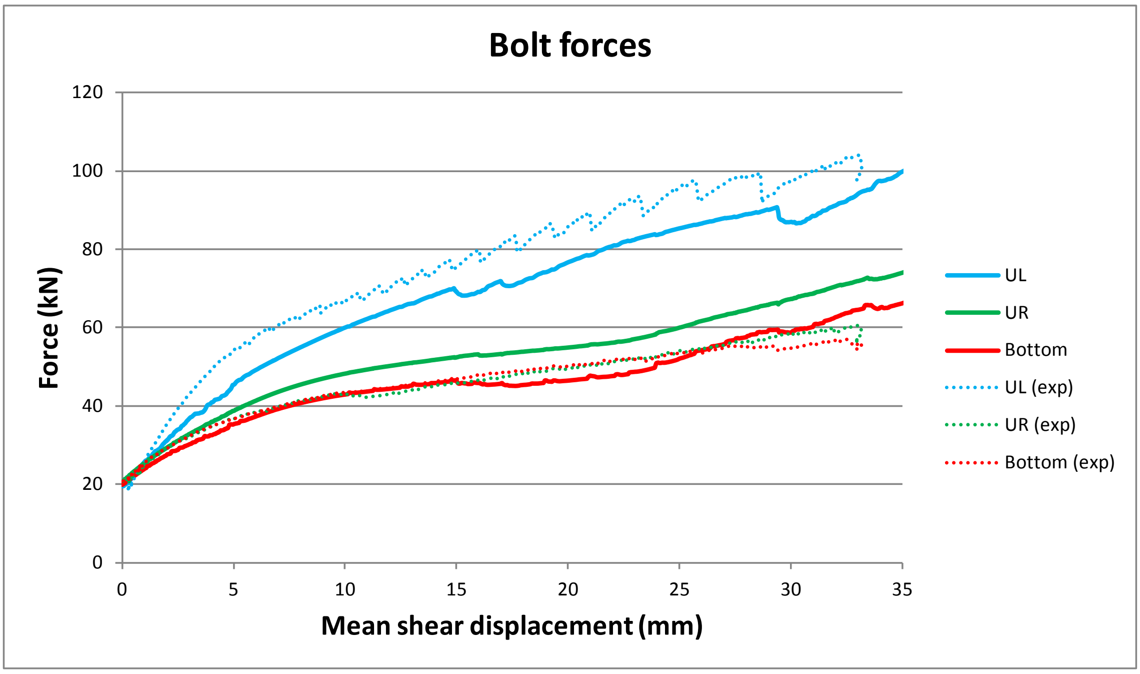

Figure 6-15. *Unmated model, strain softening rock mass: Bolt forces in kN, with experiment results indicated as dotted lines. UL = upper left, UR = upper right.*

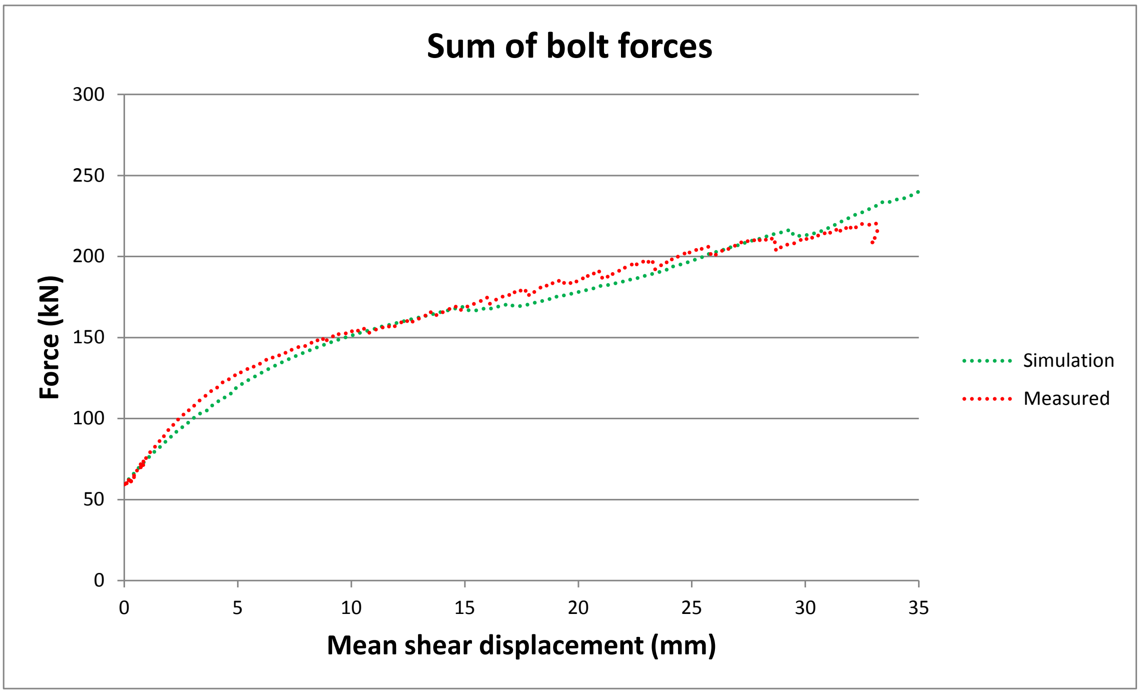

Figure 6-16. *The summed bolt forces with simulation results in green and experiment records in red from the unmated model.*

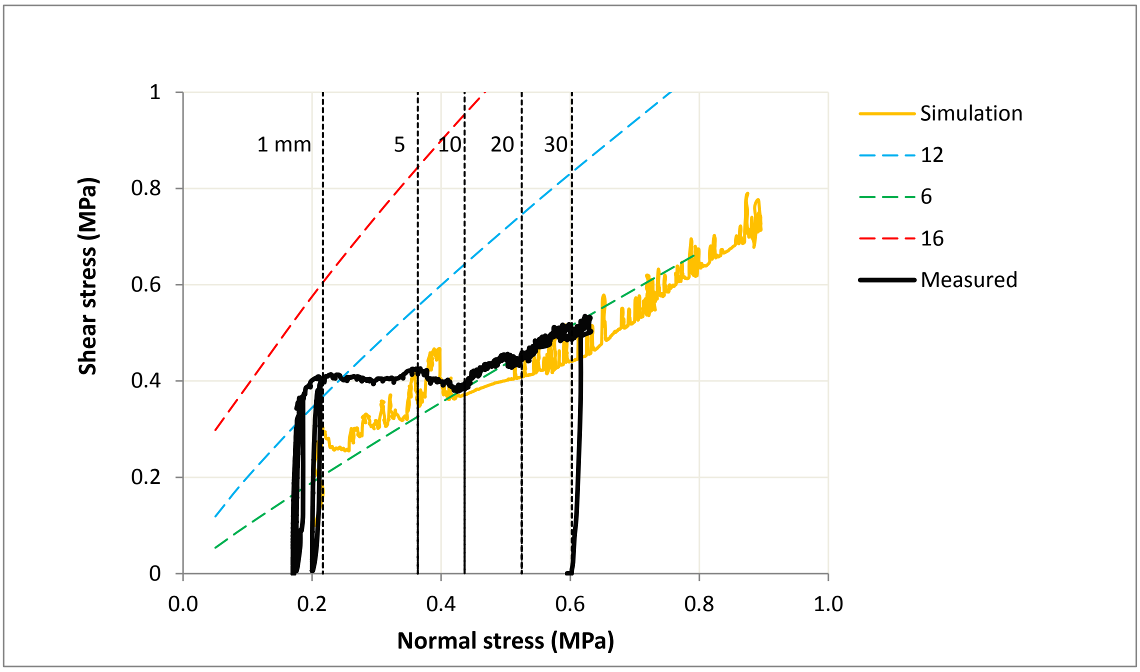

Figure 6-17. *Shear vs normal stress in MPa, with theoretical peak shear strength envelopes for JRC's of 6, 12 and 16 illustrated as green, blue and red dashed lines, respectively. Measured values plotted as a solid black line, simulation results from the unmated model in gold.*

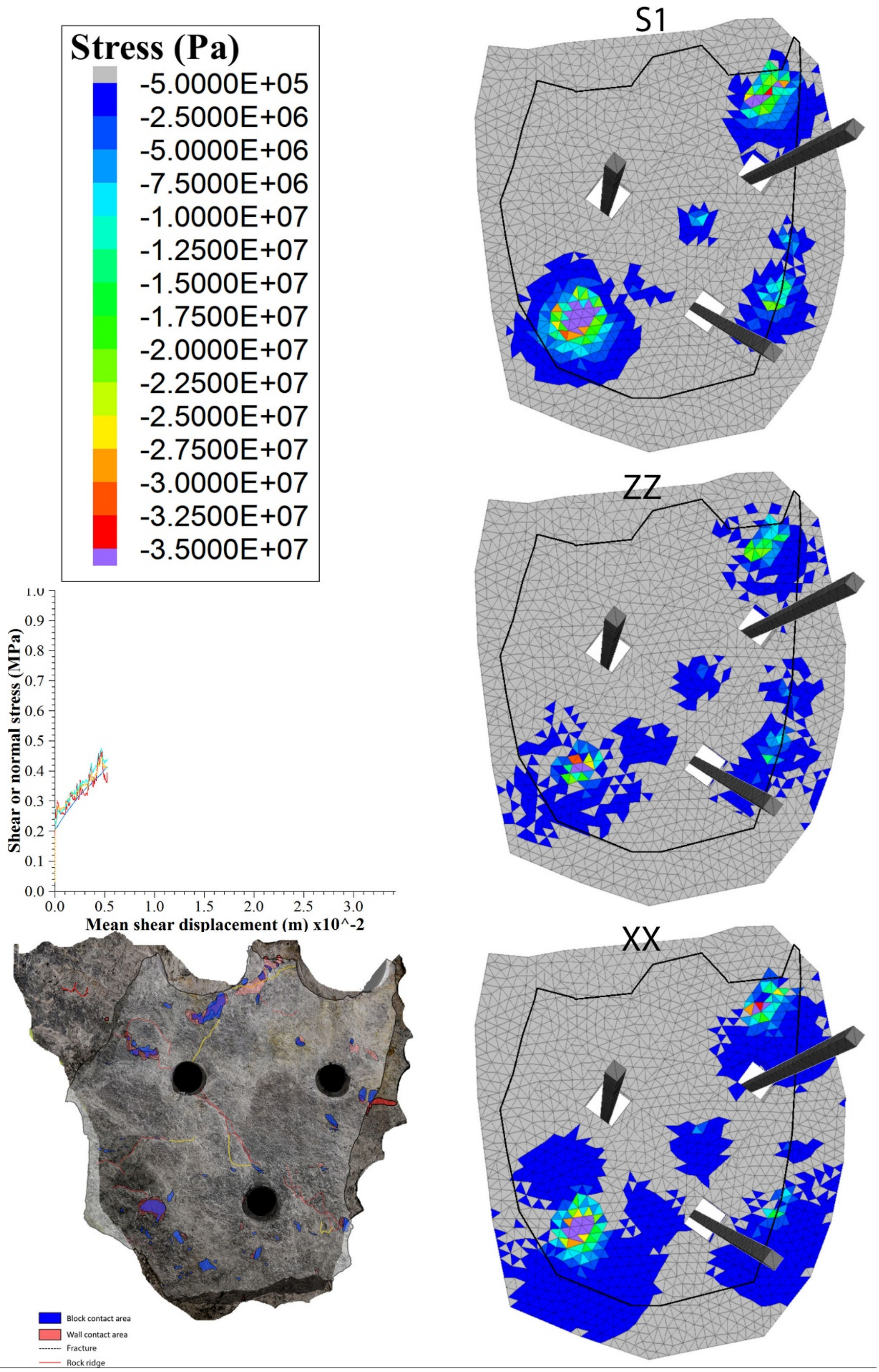

Figure 6-18. *From top to bottom after ca. 5 mm of shear displacement: σ_1, σ_{zz} and σ_{xx} contours on the fracture surface with the block outline indicated in black from the unmated model. Over 35 MPa in violet, below 50 kPa in grey.*

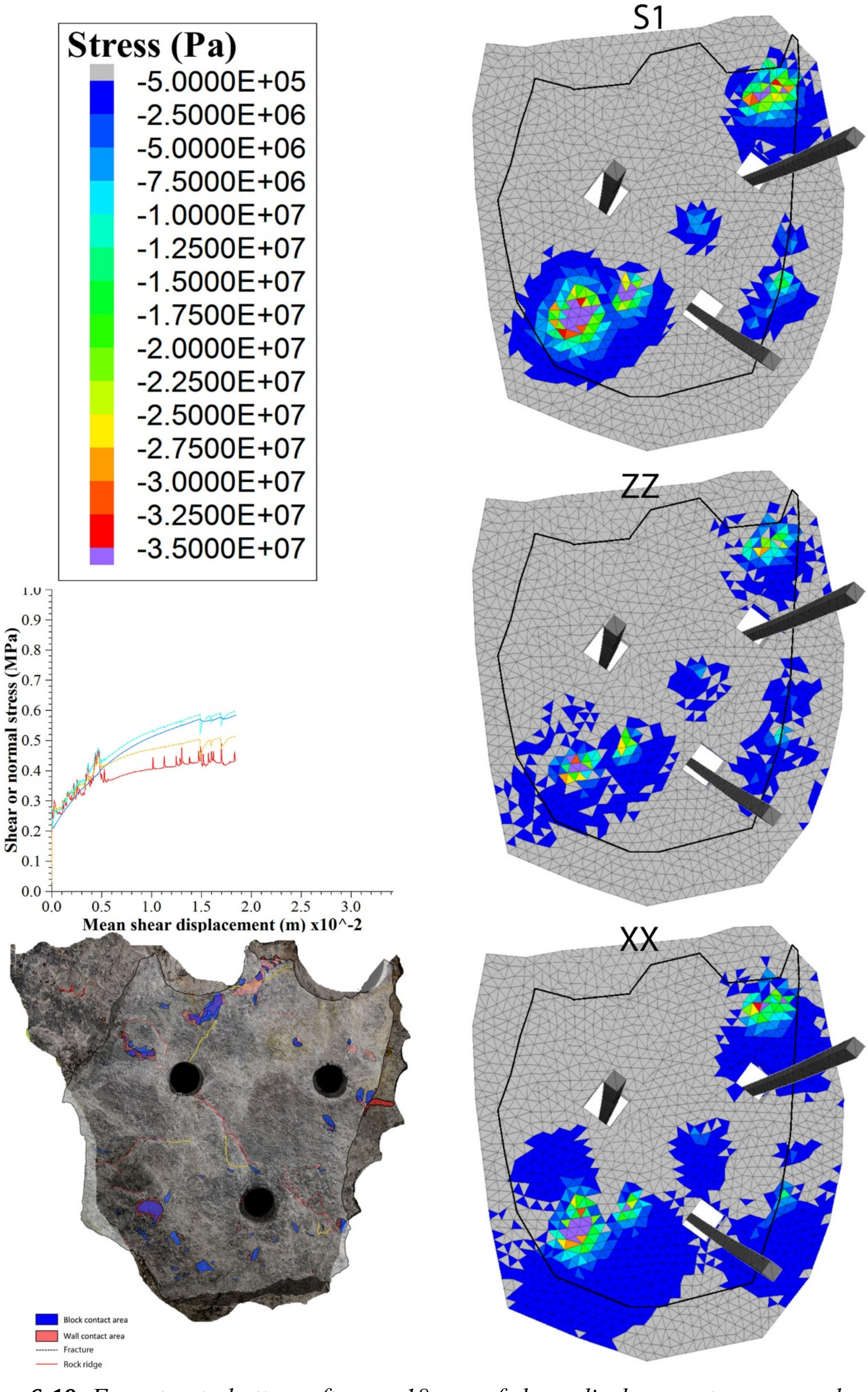

Figure 6-19. *From top to bottom after ca. 18 mm of shear displacement: σ_1, σ_{zz} and σ_{xx} contours on the fracture surface with the block outline indicated in black from the unmated model. Over 35 MPa in violet, below 50 kPa in grey.*

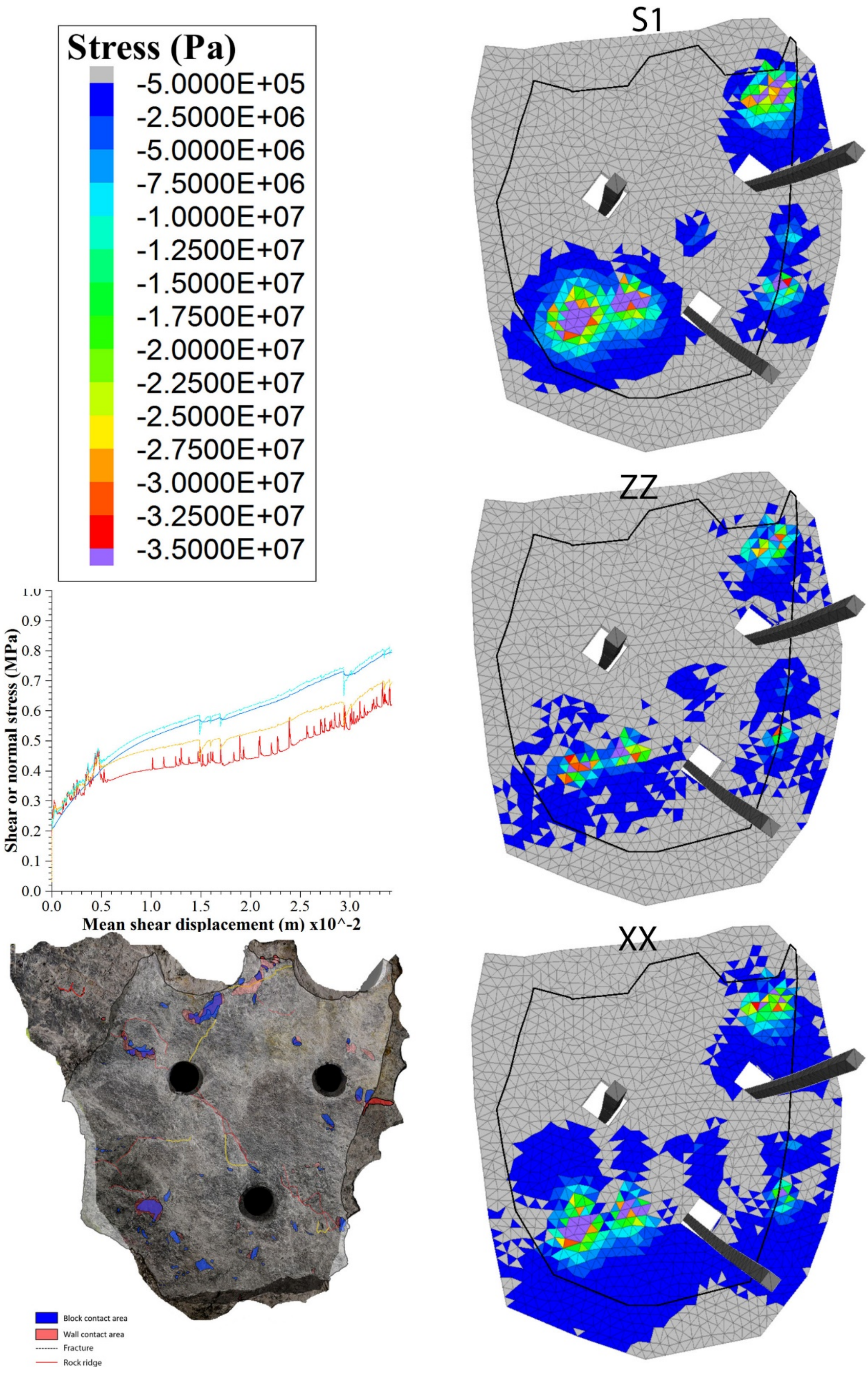

Figure 6-20. *From top to bottom after ca. 34 mm of shear displacement: σ_1, σ_{zz} and σ_{xx} contours on the fracture surface with the block outline indicated in black from the unmated model. Over 35 MPa in violet, below 50 kPa in grey.*

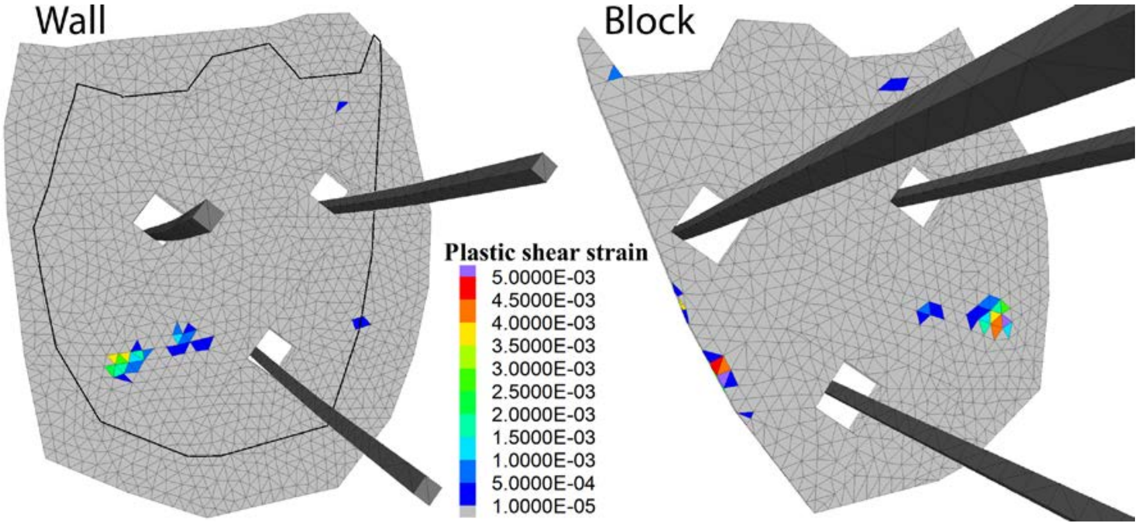

Figure 6-21. *Plastic shear strain peaks from the unmated model, observed after ca. 34 mm of displacement, from 1e-5 to 5e-3.*

It should be noted that the registered input shear force differed from the shear force registered from the fracture surfaces primarily due to the effect of fracture geometry, as shear force can be registered as normal stress (Figure 6-22).

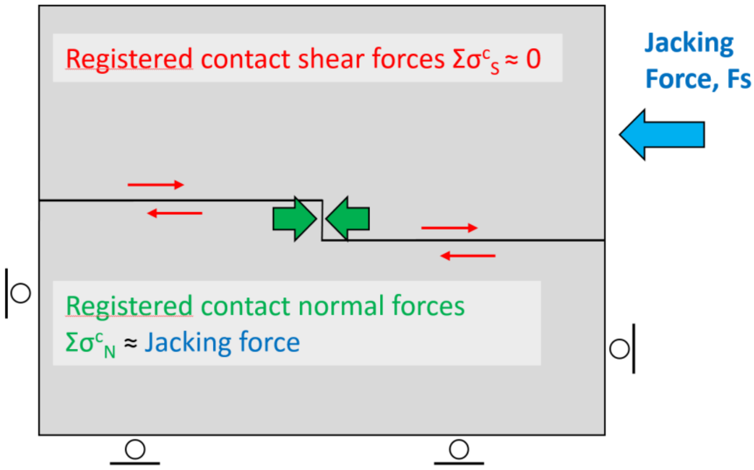

Figure 6-22. *An exaggerated illustration of how fracture surface geometry can affect registered contact force components in 3DEC i.e. the applied block shear force is registered as contact normal stress.*

7 SUMMARY AND DISCUSSION

An *in situ* PUSH test of a fracture surface under constant normal stiffness conditions was conducted at a depth of -437 meters in the ONKALO underground research facility. The objective of the experiment was to study the *in situ* shear strength of fracture surfaces at an easily accessible location, with a simple associated geometry, under low normal force and large shear displacement to gain knowledge of the shear behaviour of fractures at the site. Moreover, a series of numerical back analysis were conducted in order to understand the key mechanisms behind the observed behaviour, estimate shear strength parameters and to reveal possible test arrangement shortcomings.

The initial peaks could most likely be attributed to the part of the block in the upper left and right corners which was estimated to break approximately during the initial peak shear stresses. The discrepancy during the beginning of shear, where normal stress increased although shear stress did not, may also be attributed to this breakage. Geometrical effects i.e. local asperities could also have caused initially high shear stresses to develop prior to being sheared off. It is also notable that the fracture shear behaviour of the full block fracture surface matches a JRC of 6, which is lower than a JRC of 9, obtained from a 200 mm core through the fracture surface (section 2).

Back calculation of the experiment resulted in a fairly good match with the shear and normal stresses evaluated from jack and bolt forces during the experiment, although the initial peaks observed in shear stress could not be observed in simulations. These could only be accounted for with a densely meshed version of the model, which in this case could not be solved due to extremely long calculation times, related to the normal and shear stiffness behaviour in the CY model used within 3DEC. Note that back-analysis was performed based on shear and normal stresses originally estimated for the fracture surface (0.319 m^2): shear and normal stresses based on jack and bolt forces are 8.5% lower when using the fracture surface area obtained from photogrammetry (0.349 m^2). This does not, however, significantly affect shear strength parameters obtained through back-analysis.

Shear strength parameters were determined primarily through back-analysis which resulted in a reasonable match of observed behaviour using an initial friction angle of 47° and a residual angle of 40°. Shear and normal stiffness were found to be optimal when set to 7e-5 $\sigma_N^{1.2}$ MPa/mm and 5.1e-5 $\sigma_N^{1.014}$ MPa/mm, respectively. These parameters apply to a coarsely meshed unmated version of the fracture surface area and are possibly higher than expected as a densely meshed version of the fracture surface would have included sharp local asperities. Their expected effect would be a decrease in the initial friction angle as they would induce shear resistance in initial phases as illustrated in Figure 6-21. Most significantly, the simulation should have included the portion of the block that broke off from the upper left corner of the block which was found to be associated with the observed initial peak strength. This was partly compensated for with an increased initial friction angle. The initial contact area of the fracture was also found to be different in the simulations than in reality which could have affected shear resistance during the first few millimeters, see Section 6.1.

The interpreted initial and residual friction angles are generally over 10° higher than typical laboratory size sample values for Olkiluoto VGN, indicating that normally assumed scale effects where longer fractures exhibit a lower shear resistance may not be valid (Valli & Hakala 2016b). Most importantly a low constant normal stiffness condition was found to increase shear resistance by over 30% from the initial peak to final shear displacement of 34 mm.

The actually sheared areas of the fracture surface mapped after the test correspond to the most highly stresses areas in the coarse unmated model although the compressed areas are many times larger. A more detailed surface may produce a more realistic response. The intact rock zone size of the coarse model is far too large to yield a realistic idea of the damage exhibited by the fracture surface. Moreover, the larger elements lower the peak stresses which initiate damage.

The 3DEC simulation of an *in situ* shear test of an unmated detailed fracture surface was found challenging, but relatively good results were obtained with a coarsely modelled fracture surface exhibiting the topography relevant for large displacements. In hindsight, the densely meshed model should have been created by draping an identically triangulated grid on both fracture topographies resulting in matching gridpoints at the same locations at the beginning of shear and thereby preventing contact breaks early in shear. The drawback of this method is that it results in a smoother fracture surface than in reality and possibly removes the facing edges or asperities thought to be responsible for higher initial shear resistance.

PUSH tests of this nature would ideally be arranged so that repetition of the experiment using the same fracture surface could be arranged easily, whilst also ensuring that the following issues would not affect the experiment. A single jack was used to control both jacks and rotation of the test block was observed during the experiment. The effect of the block rotating on the results of the experiment is unknown but could have been estimated using the simulation model. As a result, it is recommended that any future setup would use individual pumps which are controlled by the displacements registered at each jack, thereby ensuring no rotation of the block during shear. The bolts were found to have bent during the test and it is unclear as to whether or not the bolt anchors had slipped or rotated. The effect of the bolts bending was estimated to be less than 4 % of the total applied shear force, when obtained from the unmated coarse model simulation based on the rebound force of the bolts upon removing the block. Avoiding bending would ideally require two I-beams installed across the block and using grouted bolts would ensure no slip occurs at the bolt anchors. Normal displacement was not measured during the test and dilation was estimated indirectly by matching simulated and measured bolt forces, which is inaccurate. Future tests should include normal displacement monitoring at three to four locations. By applying these suggestions, initial normal stress levels could be higher which would better mimic fracture shear conditions encountered in the vicinity of deep underground facilities.

Finally, PUSH tests of this nature are a valuable source of information for obtaining shear strength parameters for fractures under conditions which mimic *in situ* conditions. Ideally, similar tests with the modifications suggested above should be performed whenever possible, especially as the scale and nature of these tests are very different to those performed under laboratory conditions and back-analysis results differ significantly from conventional constant normal load laboratory test results. Suitable locations are all continuous near vertical fractures with a low angle with respect to the tunnel wall.

REFERENCES

Aaltonen, I., Engström, J., Front, K., Gehör, S., Kärki, K., Kosunen, P., Mattila, J., Paananen, M., Paulamäki, S, 2016. Geology of Olkiluoto. Posiva Report 2016-16. Posiva Oy, Eurajoki, Finland.

Barton, N. & Choubey, V. 1977. The shear strength of rock joints in theory and practice. Rock Mechanics 1/2:1-54. Vienna: Springer.

Barton, N. 2002. Some new Q-value correlations to assist in site characterisation and tunnel design. International Journal of Rock Mechanics and Mining Sciences 39 (2002), 185–216.

Diederichs, M. Carter, T., and Martin, D. 2010. Practical Rock Spall Prediction in Tunnels. ITA World Tunnel Congress Vancouver, 2010.

Hakala, M., Siren, T., Kemppainen, K., Christiansson, R. & Martin, D. 2013. In Situ Stress Measurement with the New LVDT-cell – Method Description and Verification. Posiva Report 2012–43. Posiva Oy, 180 p.

Itasca 2016. *Software: 3DEC.* Accessed 28 September 2016. http://www.itascacg.com/3dec

Jacobsson, L., Flansbjer, M., Andersson, L., Appelquist, K., 2016. Normal loading and shear tests on rock joints from Olkiluoto. Working Report 2016-30. Posiva Oy.

Johansson, Fredrik. 2015. Influence of scale and matedness on the peak shear strength of fresh, unweathered rock joints. International Journal of Rock Mechanics and Mining Sciences 82 (2016), 36 – 47.

Posiva 2013. Olkiluoto site description 2011. Report POSIVA 2011-02. Posiva Oy, Eurajoki, Finland.

Siren, T., Christiansson, R., Lam, T., Hakala, M., Valli, J., Mas Ivars, D., Mattila, J. 2016. Parametrisation of Fractures - Final report. Posiva Report xxx (due 2016).

Valli, J. & Hakala, M. 2016a. Parametrisation of Fractures – Model generation methodology and prediction calculations Working Report 2016-32. Posiva Oy, Eurajoki, Finland.

Valli, J. & Hakala, M. 2016b. ONKALO POSE Experiment - Analysis Of Rock Mechanics Test Data. Working Report 2016-49. Posiva Oy, Eurajoki, Finland.

Wilson, J. S. 2005. Sensor Technology Handbook. Elsevier Inc., 380–381.